Received June 2, 2021, accepted June 19, 2021, date of publication June 25, 2021, date of current version July 6, 2021.

Digital Object Identifier 10.1109/ACCESS.2021.3092529

A Review of Sparse Sensor Arrays for Two-Dimensional Direction-of-Arrival Estimation

IBRAHIM ABOUMAHMOUD, ALI MUQAIBEL, (Senior Member, IEEE), MOHAMMAD ALHASSOUN, (Member, IEEE), AND SALEH ALAWSH, (Member, IEEE)

Electrical Engineering Department, King Fahd University of Petroleum and Minerals, Dhahran 31261, Saudi Arabia
Center for Communication Systems and Sensing, King Fahd University of Petroleum and Minerals, Dhahran 31261, Saudi Arabia

Corresponding author: Ali Muqaibel (muqaibel@kfupm.edu.sa)

This work was supported by the Deanship of Scientific Research, King Fahd University of Petroleum and Minerals (KFUPM), under Grant SB191009.

This work did not involve human subject or animals in its research.

ABSTRACT Two-dimensional (2D) arrays are fundamental to localization applications. Specifically, sparse arrays can provide superior direction-of-arrival (DoA) estimation performance with limited number of sensors. There has been increased interest in the research community in designing 2D sparse arrays with performance improvement and complexity reduction. The research efforts are uncoordinated resulting in some repetitions and sometimes conflicting claims. After introducing 2D sparse arrays and their importance, this paper establishes the 2D-DoA estimation model and consolidates the performance metrics. An extensive literature overview of sparse arrays for 2D-DoA estimation is presented with an attempt to categorize existing works. The examined arrays include parallel arrays, L-shaped, V-shaped, hourglass, thermos, nested planer, and coprime planner, to name a few. Existing designs are compared in terms of required number of sensors, degrees of freedom (DOF), algorithm used, associated complexity and aperture size. The focus is on describing the sparse arrays, yet some specific details on DoA estimation algorithms are provided for selected array geometries. Fundamental problems of 2D-DoA estimation are outlined and existing solutions to alleviate these problems are discussed. This should be useful in predicting the estimation performance and required complexity; thus, aiding the decision of selecting a sensor geometry for DoA estimation. This review serves as a starting point for researchers interested in exploring or designing new 2D sparse arrays. It also helps to identify the gaps in the field and avoids unnecessary minor design modifications.

INDEX TERMS Antenna arrays, array signal processing, direction-of-arrival estimation, 2D-DoA estimation, planar arrays, sensor arrays, sparse arrays.

I. INTRODUCTION

direction-of-arrival (DoA) estimation is an important application of array signal processing that has received increasing interest in the past decades.

It is widely used in radio frequency and acoustics domains with similar array design and processing concepts. The performance and accuracy of the estimation algorithms are usually affected by some factors such as the coherence of sources, distribution of noise, signal-to-noise ratio (SNR), and the geometry of the sensor array. DoA estimation has proved useful in applications like sonar and radar [1]. It is also finding many applications in new generations of wireless communications and multiple input multiple output systems [2]–[4].

Various sensor arrays have been studied previously for DoA estimation like one-dimensional (1D) linear arrays (LAs), and two-dimensional (2D) planar arrays. An essential property of a sensor array is its *resolution capacity*, i.e. the maximum number of resolvable waves impinging on the array [5], [6]. For many years, the linear equispaced array (LES) [7], more commonly known as the uniform linear array (ULA) was paramount for the development of DoA estimation algorithms. For a ULA with N_t omnidirectional elements, and with the assumptions of narrow-band sources, having the same carrier frequency, with full-rank sample correlation matrix (of sources amplitudes), a full-rank correlation matrix of sensor outputs, and inter-sensor spacing less than or equal

The associate editor coordinating the review of this manuscript and approving it for publication was Chengpeng Hao.

to half signal wavelength (λ), it was known that $N_t - 1$ sources can be resolved [6]. This limit, however, was exceeded using methods employing higher order statistics like the fourth order cumulants (FOC), which has the capability of eliminating Gaussian noise, but obviously, cannot work if the sources are also Gaussian [8], [9]. A different approach for increasing the resolution capacity of linear arrays focused on reducing the redundancy of inter-sensor[1] spacing, which opened the realm of sparse sensor arrays, i.e. arrays that have non-uniform inter-sensor spacings but are integer multiple of a fundamental distance, $d = \lambda/2$.

For linear arrays, it is known that only four arrays exhibit zero-redundancy, i.e. each inter-sensor spacing occurs once for all elements in the array, and the largest zero-redundancy array has only four sensors [10]. An easy way to list these four arrays is on a number line, thus the first zero-redundancy array has sensors at $\{0\}$, the second at $\{0, 1\}$, the third at $\{0, 1, 3\}$, and the fourth at $\{0, 1, 4, 6\}$. Due to the limited number of sensors with zero-redundancy, researchers focused on finding minimum redundancy arrays (MRAs), previously called linear minimum redundancy (LMR) arrays [10]. Finding and using MRAs for direction finding is a challenging task, since locations of antenna elements does not have a closed-form expression, and are found using complicated approaches [5], [11], [12]. Other sensor arrays were developed over the last few decades including *Wichmann* [13], *coprime* [14], [15], *multi-level prime* [16], *nested* [17], *super nested* [18], and *cantor* [19] arrays, among others.

In terms of space and power budget, sparse arrays are valuable as they can reduce the cost, or increase the performance for the same cost. The array geometry plays a key role in the direction finding performance and capability. In the literature, 1D antenna arrays have been used extensively. A nice comparison for the three linear sparse arrays: *Wichmann* [13], *nested* [17], and *super nested* [18] arrays was published in 2017 by Rajamäki and Koivunen [20]. The article focused on deriving expressions for the maximum aperture, and comparing the performance of these arrays with the optimal MRA. Another work by Alawsh and Muqaibel [16] compared the *coprime* [14], [15], *Nested* [17], and *Super nested* [18] arrays with *multi-level prime array*, which is an extension of the coprime array, and they also compared with a *compressed multi-level prime array* in terms of DoA estimation performance under mutual coupling considering multiple signal classification (MUSIC) algorithm and sparse reconstruction algorithms. However, the two studies above are limited to 1D arrays.

There is a growing interest in 2D and three-dimensional (3D) arrays that usually result in a much finer location resolution. Mazlout et al. [21] presented a comparison between the uniform rectangular array (URA) and the L-shaped array (made up of two orthogonal ULAs sharing a single sensor). Nonetheless, they considered only two arrays that are not sparse (refer to the discussion in Section III-B1). Another very thorough review for 1D and 2D-DoA estimation was published in 2010 by Gershman et al. [22]. It covered the fundamental concepts and focused on search-free techniques, and algorithms that work for arbitrary arrays, which include uniform and sparse arrays. On the general topic of estimation in signal processing, Zoubir *et al.* [23] presented a tutorial which includes valuable information on DoA estimation, but does not describe specific array geometries. There are also less related comparison studies by Adhikari and Drozdenko [24]–[27], and reviews in other areas related to DoA estimation [28], [29].

Most of the published work is generally concerned with DoA estimation of sources in the far-field. That is, sources far away from the Fresnel region of the antenna array. There is also 3D-DoA estimation, which is concerned with finding DoA and range for sources in the near-field of the array. In fact, the far-field regime can be considered as an extension of the near-field one, with infinite range.

In the last decade, there has been a growing interest in designing specific 2D array geometries and developing specific 2D-DoA estimation algorithms for them, which tend to show superior performance compared to algorithms that work with arbitrary sensor array geometries. There is no clear structures in the development strategies as more and more structure appear. This manuscript aims to put all previous work in perspective and provides an overview of 2D sparse sensor geometries that go in tandem with special DoA estimation algorithms, which can therefore surpass the performance of arbitrary sparse sensor geometries with generic DoA estimation algorithms. This review helps to identify the gaps in the field and to avoid unnecessary minor modifications. To the best of the authors' knowledge, the considered focus and geometries were not collectively presented in a single work before. The rest of this manuscript is organized as follows: the essentials of 2D-DoA estimation are explored in Section II. Then, Section III describes notable 2D sparse geometries [30]–[64] for DoA estimation, and some details on the DoA estimation algorithm are outlined for selected arrays. Concluding remarks are drawn in Section V.

The following mathematical notations are used: for a matrix $\mathbf{A}$, $\mathbf{A}^*$ is its complex conjugate, $\mathbf{A}^T$ is its transpose, and $\mathbf{A}^H$ is its Hermitian. The operator $\mathbb{E}$ is the expectation operator, $\otimes$ is the Kronecker product, $\odot$ is the Khatri-Rao product, $\lfloor x \rfloor$ is the floor of x, bold-face lower-case letters (e.g., $\mathbf{a}$) stand for vectors, bold-face upper-case letters (e.g., $\mathbf{A}$) stand for matrices, and the overhead hat (as in $\hat{\theta}$) denotes the estimated version of the variable below it.

II. TWO-DIMENSIONAL DoA ESTIMATION ESSENTIALS

A 2D-DoA estimation problem can be decomposed into two separate 1D-DoA estimation problems, where some 1D algorithms can be utilized. When the 2D estimation problem is decomposed into two linear problems, automatic pairing of angles is an advantage, as this usually means less complexity and better estimates [65], [66]. In the research literature,

[1] In this article, the word sensor refers to the element of the array; thus, sensors and array elements are used interchangeably.

several well-established algorithms for 1D direction finding are used such as MUSIC [67] and estimation of signal parameters via rotational invariance techniques (ESPRIT) [68]. However, real-time analysis often requires faster algorithms that do not require either singular-value decomposition (SVD) or eigen-value decomposition (EVD). Usually, search-free algorithms are faster than subspace methods [22]. An example of an algorithm that does not require SVD or EVD is the propagator method (PM) which employs least-squares on the received covariance matrix [69]. The use of extended versions of these algorithms can be found in many works. For example, 2D MUSIC was reported in [70], 2D ESPRIT in [66], [71], [72], and the PM in [73]–[76]. The following general questions are important in characterizing any 2D-DoA estimation algorithm, some of them are borrowed from the 1D case:

- Can the method resolve more signals than the number of physical sensors? which is valuable in numerous cases [77].
- Are the available physical sensors fully utilized? That is, sensors are not underutilized or non-essential [19], [78]. For instance, algorithms based on PM usually only resolve sources less than half the number of physical sensors [30].
- What are the ranges of angles the 2D algorithm successfully covers? For instance, some algorithms fail for high elevation angles [74].
- Can the sensor array perform well in real conditions? for example in presence of mutual coupling [54] and model mismatch [79], [80]. Also is it robust to sensor failure? [81], [82]

Generally, the aperture of the array is directly related to the maximum number of resolvable sources, and the inter-sensor spacing is related to possible aliasing of some angle estimates; more details in [27] and references therein. If the linear sparse array can provide the same main lobe beamwidth as a ULA, then it should be able to resolve the same number of sources as the ULA. Alternatively, if the linear sparse array has a continuous (hole-free) coarray (i.e. the coarray is a ULA), then it should be able to resolve the same number of sources as a ULA similar to the coarray [27]. Similar ideas are used for 2D-DoA estimation, where it is preferred to get as close as possible to uniform rectangular coarray. The next subsections briefly mention the system model for 2D-DoA estimation, then explore the coarray concept, a useful mathematical property that is utilized in many DoA estimation algorithms.

A. 2D SYSTEM MODEL

The 2D system model describes the signals emerging from the sources to be localized, the antenna array, and the employed signal processing to extract features of interest. The signals can be in the far-field or the near-field, polarized or non-polarized, coherent or incoherent, correlated or uncorrelated. The sensor array could be 1D, 2D, or 3D, uniform or sparse or neither (see Section III). The sensors can be omnidirectional or directional, polarized or non-polarized. The features to be estimated could be the 1D-DoA, or 2D-DoA, polarization, or range (distance to the source). The previous scenarios are certainly not comprehensive and extra considerations are required for practical implementations. For instance, mutual coupling, sensor failure, array calibration, and sensor characteristics mismatch are some physical hindrances for successful deployment of a functioning system.

An example of nine-element URA is shown in the $x-y$ plane of Fig. 1 to illustrate important geometrical variables. The following symbols are used across this document, and the meaning mentioned here is assumed unless otherwise noted.

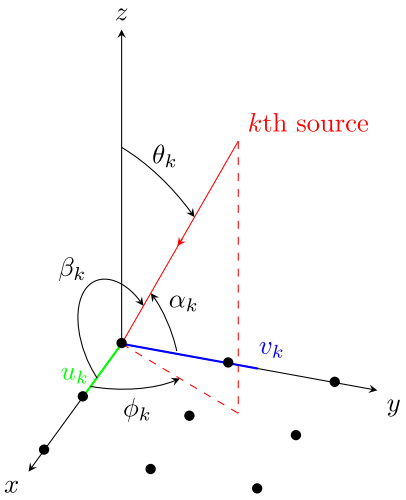

FIGURE 1. A nine-element URA example to illustrate important geometrical variables.

- T is the number of snapshots,
- K is the number of narrow-band impinging sources and k is used for the kth source (i.e. $k = 1, 2, \ldots, K$),
- N_i and M_i are used for the number of antenna elements in the linear subarray i (the exact meaning is clarified for each antenna array geometry),
- N_t is the total number of physical sensors in the array,
- d_x is the fundamental spacing along the x-axis, d_y is the fundamental spacing along the y-axis, often $d_x = d_y$,
- $\phi_k \in [0, 2\pi]$ is the azimuth angle of the kth source (measured from the positive x-axis), $\theta_k \in [0, \pi]$ is the elevation angle (measured from the positive z-axis); these angles are illustrated in Fig. 1,
- $\alpha_k \in [0, \pi]$ is the angle between the line connecting kth source with the origin and the positive y-axis, $\beta_k \in [0, \pi]$ is the angle between the line connecting kth source with the origin and the positive x-axis.

In addition, the following *direction cosines* are used by some authors to simplify expressions

$$u_k := \cos(\beta_k) := \sin(\theta_k)\cos(\phi_k), \tag{1}$$

$$v_k := \cos(\alpha_k) := \sin(\theta_k)\sin(\phi_k), \tag{2}$$

where α_k and β_k are called electric angles, and they simplify many analytical expressions since they can be separated from each other. Other used geometrical variables are [54]

$$\bar{\theta}_k := \frac{d}{\lambda}\sin(\theta_k)\cos(\phi_k), \tag{3}$$

$$\bar{\phi}_k := \frac{d}{\lambda}\sin(\theta_k)\sin(\phi_k). \tag{4}$$

Apart from variables that depend on the sensor array geometry (N_i, M_i, d_x and d_y), the rest of the variables are shown in Fig. 1. While this work tries to unify the notation in the majority of existing works, several differences remain present, and Table 1 shows some differences comparing other works to the selected notation.

TABLE 1. Mapping between some symbols in cited papers and their equivalent in this document.

Ref.	Symbol	Equiv. Symbol
[55]	ϕ, θ	θ, ϕ
[30, 31, 34, 35, 42, 43, 52, 57]	M, N	M_1, M_2
[31, 32]	$\mathbb{L}$	$\mathbb{S}$

Consider a system for estimating the 2D-DoA of far-field non-polarized signals. When a single source is considered, the sampled output of the sensor array at a time instant t can be written as [54], [67], [83]

$$\mathbf{x}(t) = \mathbf{a}(\theta_k, \phi_k)s(t) + \mathbf{n}(t), \tag{5}$$

where $\mathbf{a}(\theta_k, \phi_k) \in \mathbb{C}^{N_t \times 1}$ is the array manifold (or steering vector) with entries $e^{j2\pi(\bar{\theta}_k p_x + \bar{\phi}_k p_y)}$ for all $(p_x, p_y) \in \mathbb{S}$ and $\mathbb{S}$ is the set of sensor locations, $s(t)$ is the transmitted signal, $\mathbf{x}(t) \in \mathbb{C}^{N_t \times 1}$ for N_t sensors, and $\mathbf{n}(t) \in \mathbb{C}^{N_t \times 1}$ is the additive noise vector, that is often assumed to be spatially and temporally white Gaussian noise and uncorrelated at each array element, that is $\mathbb{E}[\mathbf{n}(t)\mathbf{n}^H(t)] = \sigma^2\mathbf{I}$, where σ^2 is the noise power and $\mathbf{I}$ is the identity matrix.

When more sources are considered, the model can be written as

$$\begin{bmatrix} x_1(t) \\ x_2(t) \\ x_3(t) \\ \vdots \\ x_{N_t}(t) \end{bmatrix} = \begin{bmatrix} & & \\ \mathbf{a}(\theta_1, \phi_1) & \dots & \mathbf{a}(\theta_K, \phi_K) \\ & & \end{bmatrix} \times \begin{bmatrix} s_1(t) \\ s_2(t) \\ \vdots \\ s_K(t) \end{bmatrix} + \begin{bmatrix} n_1(t) \\ n_2(t) \\ n_3(t) \\ \vdots \\ n_{N_t}(t) \end{bmatrix} \tag{6}$$

Then taking T time samples (snapshots), the model can be written compactly as

$$\mathbf{X} = \mathbf{AS} + \mathbf{N} \tag{7}$$

where $\mathbf{X} \in \mathbb{C}^{N_t \times T}$, $\mathbf{A} \in \mathbb{C}^{N_t \times K}$, $\mathbf{S} \in \mathbb{C}^{K \times T}$, $\mathbf{N} \in \mathbb{C}^{N_t \times T}$.

The source is considered in the far-field if it lies beyond the Fraunhofer distance, $2D^2/\lambda$, where D is the aperture of the array, and λ is the wavelength of the source [53], [84]. If the source range is less than this limit, it is considered in the near-field.

B. TERMINOLOGY OF 2D ARRAYS

This section is a necessary extension to the previous one. It explains the set of array elements $\mathbb{S}$ and how mutual coupling is modeled. Since this work considers 2D sensor arrays which can be represented in a rectangular grid (except the V-shaped array, Section III-B3), it is convenient to describe the sensor locations as integers, where it is understood that the fundamental unit is d: the fundamental (minimum) distance between any pair of sensors, which is often chosen as $d = \lambda/2$. The set of sensor elements is denoted by $\mathbb{S}$ in this work. Note that other authors using this set might call it $\mathbb{L}$ for example [31], [32], as noted in Table 1.

Mutual coupling is usually modeled by a mutual coupling matrix (MCM) $\mathbf{C} \in \mathbb{C}^{N_t \times N_t}$ that is multiplied by the array manifold matrix (AMM) $\mathbf{A} \in \mathbb{C}^{N_t \times K}$. Technically, the MCM should be specific to each set of antennas, taking into consideration the physical dimensions of the antennas and feeding points [79]. Usually, antenna spacing is the dominant factor. In fact, it was empirically observed that the behavior of the MCM is approximately a function of sensor separations only [18]. In two dimensions, the MCM can be assumed to be a B-banded symmetric Toeplitz matrix [54], [63], [85]

$$\langle \mathbf{C} \rangle_{\mathbf{p}_1, \mathbf{p}_2} = \begin{cases} c\left(\|\mathbf{p}_1 - \mathbf{p}_2\|_2\right), & \text{if } \|\mathbf{p}_1 - \mathbf{p}_2\|_2 < B \\ 0, & \text{otherwise} \end{cases} \tag{8}$$

where $\langle \mathbf{C} \rangle_{\mathbf{p}_1, \mathbf{p}_2}$ denotes the value of $\mathbf{C}$ at a sensor pair $\mathbf{p}_1$, $\mathbf{p}_2 \in \mathbb{S}$, $\|\cdot\|_2$ is the ℓ_2-norm, B is the maximum separation between coupled sensors, and $c(\cdot)$ denotes the mutual coupling coefficient. In addition, it is assumed that

$$c(0) = 1, \quad \& \quad \left|\frac{c(k)}{c(\ell)}\right| = \frac{\ell}{k}, \quad \text{for } k, \ell > 0 \tag{9}$$

C. COARRAY

An essential step employed in most DoA estimation algorithms with sparse arrays is finding the coarray of the physical array. For the case of non-coherent sources, the difference coarray is of interest, and is defined as follows [77].

Definition 1 (Difference Coarray): If a set $\mathbb{S}$ denotes the set of ordered pairs of points representing the coordinates of physical sensors in a sensor array, then the difference coarray set is given by

$$\mathbb{D} = \{\mathbf{m} | \mathbf{m} = \mathbf{p}_1 - \mathbf{p}_2, \forall \mathbf{p}_1, \mathbf{p}_2 \in \mathbb{S}\}. \tag{10}$$

Alternatively, $\mathbf{p}_1$ and $\mathbf{p}_2$ can be considered as vectors in $\mathbb{R}^{2\times 1}$ denoting physical sensor locations. The maximum number of virtual sensor elements in the coarray is $N_t(N_t - 1) + 1$, regardless of the array geometry [17]. The difference coarray sensors are symmetric with respect to the origin, and

it is important since it appears naturally in the cross correlation between two sensors in the array, i.e. when second order statistics (SOS) are used, which is an equivalent representation of virtual sensors at the locations of the differences [59]. Another widely used term for the coarray is the holes, which can be defined as follows

Definition 2 (Hole-Free Coarray): If a set $\mathbb{D}$ denotes a coarray on a rectangular integer grid, and the minimum and maximum elements are denoted as $\min \mathbb{D}$ and $\max \mathbb{D}$. If all possible combinations of pairs in $[\min \mathbb{D}, \max \mathbb{D}]$ exist in the coarray, then the coarray is hole-free. Alternatively, if $\mathbb{U}$ denotes a URA which includes the origin, and $\mathbb{D} = \mathbb{U}$, then $\mathbb{D}$ is hole-free.

This definition implies that any element in $\mathbb{U}$ but not' in $\mathbb{D}$ is a hole. It is often desirable to get a continuous (hole-free) coarray, i.e. a ULA for linear arrays or a URA for planar arrays. Reasons include: Better identifiability of DoAs using estimation algorithms like MUSIC with spacial smoothing [15], [17] ; and $\mathcal{O}(N_t^2)$ uncorrelated DoAs can be identified with a coarray of $\mathcal{O}(N_t^2)$ sensors. In 2D, this holds only almost surely [54], [86]. In general, if the elements of a coarray are continuous on a uniform rectangular grid, then the coarray is hole-free. It is possible to extend the hole-free definition to the 3D arrays [54]. An important definition for the coarray is the weight function, which gives an insight on the significance of mutual coupling on DoA estimation [18], [54].

Definition 3 (Weight Function): If a set $\mathbb{S}$ denotes the set of physical sensors' positions in a sensor array, and $\mathbb{D}$ denotes the difference coarray, then

$$w(\mathbf{m}) = w(m_x, m_y) = \left|\{(\mathbf{p}_1, \mathbf{p}_2) \in \mathbb{S}^2 | \mathbf{p}_1 - \mathbf{p}_2 = \mathbf{m}\}\right| \quad (11)$$

denotes the number of sensor pairs with separation $\mathbf{m} \in \mathbb{D}$. Note that $\mathbf{m} = (m_x, m_y)$ is a two-component vector, and $|\cdot|$ denotes the cardinality.

For example, the most significant weights are $w(0, 1)$, $w(1, 0)$, and then $w(1, 1)$, $w(1, -1)$, since the first two count the elements with unity inter-sensor spacing, and the other two for $\sqrt{2}$ inter-sensor spacing (of course scaling factors d_x and d_y are neglected). The first two weights mean the number of sensors having inter-element spacing of unity, which is the smallest possible inter-sensor spacing. The difference is just which axis this weight is calculated across. An array geometry with the less value for $w(0, 1)$, $w(1, 0)$, $w(1, 1)$, and $w(1, -1)$ is usually less susceptible to mutual coupling degradation in DoA performance.

D. PERFORMANCE METRICS

Many performance metrics have been utilized to assess the performance of 2D-DoA estimation algorithms. This includes computing the deviation (error) from the known DoA; where the root mean square error (RMSE) is the most widely used metric [31]–[38], [40]–[58], [60]–[63]. However, other metrics can be used like the mean square angular error (MSAE) [87], mean square error (MSE) [88], and maximum root mean square error (MRMSE) [89]. In addition, when the 2D-DoA algorithm is expected to work in the underdetermined case, i.e. when estimating more sources than the available sensors, it is insightful to compare the degrees of freedom (DOF) offered by the 2D-DoA estimation algorithms, the coarray, and the aperture. Furthermore, the computational complexity or running time and probability measures for success (correct resolution) or failure can be employed. This subsection highlights some performance metrics that are commonly utilized.

1) ROOT MEAN SQUARE ERROR (RMSE)

For 2D-DoA estimation, the RMSE usually considers both azimuth and elevation angles [44], [47], [61], [62], [90]

$$\text{RMSE} = \sqrt{\frac{1}{HK}\sum_{h=1}^{H}\sum_{k=1}^{K}\left((\theta_k - \hat{\theta}_{k,h})^2 + (\phi_k - \hat{\phi}_{k,h})^2\right)} \quad (12)$$

where H is the number of Monte-Carlo trials. However, some authors still compute separate errors for azimuth and elevation angles [35], [50]

$$\text{RMSE}_\theta = \sqrt{\frac{1}{HK}\sum_{h=1}^{H}\sum_{k=1}^{K}\left((\theta_k - \hat{\theta}_{k,h})^2\right)} \quad (13)$$

$$\text{RMSE}_\phi = \sqrt{\frac{1}{HK}\sum_{h=1}^{H}\sum_{k=1}^{K}\left((\phi_k - \hat{\phi}_{k,h})^2\right)} \quad (14)$$

The RMSE can also be calculated based on the electrical angles α_k and β_k. Note that many variations exist in the literature like dividing by K outside the square root instead of inside [32], dividing by $2HK$ instead of HK [43], [49], [52], keeping the averaging over sources outside the square root [45], or defining the RMSE keeping only the averaging over sources inside the square root and then average Monte-Carlo trials [54], [63].

2) COARRAY PROPERTIES

As discussed earlier, the coarray is preferred to be hole-free, that is, all virtual elements in the coarray are contiguous. If this is not the case, then some properties are considered like the number of unique lags, n_{ul}

$$n_{ul} = |\mathbb{D}| \quad (15)$$

In addition, the contiguous URA portion of a coarray can be determined by finding the longest contiguous ULA on the x-axis $\mathbb{D}_{x\text{ULA}}$ and the longest contiguous ULA on the y-axis $\mathbb{D}_{y\text{ULA}}$, then multiplying the number of elements in $\mathbb{D}_{x\text{ULA}}$ and $\mathbb{D}_{y\text{ULA}}$ to find the number of consecutive lags, n_{cl}

$$n_{cl} = |\mathbb{D}_{x\text{ULA}}| \times |\mathbb{D}_{y\text{ULA}}| \quad (16)$$

Note that the two virtual ULAs $\mathbb{D}_{x\text{ULA}}$ and $\mathbb{D}_{y\text{ULA}}$ are symmetric about the origin since the coarray is. It is possible, however, to consider consecutive lags on other

contiguous URAs (if they exist), but those are usually smaller than the consecutive URA that includes the origin. The weight function is another coarray property that is also considered for evaluating a sensor array.

3) REDUNDANCY

When all elements in the coarray appear exactly once, the sensor array is said to have unity redundancy, i.e. $R = 1$. Usually, sensor arrays with contiguous (hole-free) coarrays have $R > 1$. The asymptotic redundancy $R_\infty = \lim_{N_t \to \infty}$ can be used to compare sparse sensor arrays [64].

4) SPARSENESS

Unlike the weight function, sparseness (S) counts the sensor pairs separated by a positive distance $\tilde{d}$ [64]

$$S(\tilde{d}) = \frac{1}{2} \sum_{\mathbf{m} \in \mathbb{D}} v_\Delta(\mathbf{m}) \cdot \mathbb{1}\left(\|\mathbf{m}\|_2 = \tilde{d} \right) \tag{17}$$

where $v_\Delta(\mathbf{m}) = \sum_{\mathbf{p}_1, \mathbf{p}_2 \in \mathbb{S}} \mathbb{1}(\mathbf{m} = \mathbf{p}_1 - \mathbf{p}_2)$ is the multiplicity function (analogous to the weight function) for the difference coarray and $\mathbb{1}(\cdot)$ is the indicator function. For instance, for a sensor array on a uniform grid, $\tilde{d} \in \{1, \sqrt{2}, 2, \sqrt{5}, \sqrt{8}, 3, \dots\}$. Alternatively, sparseness can be viewed as the summation of essential weight function pairs with the same absolute distance. For example, $S(1) = w(1, 0) + w(0, 1)$, $S(\sqrt{2}) = w(1, 1) + w(1, -1)$, etc. In other words, sparseness abstracts dimension-specific weight values.

5) COUPLING LEAKAGE

Coupling leakage, $\mathcal{L} \in [0, 1]$ quantifies the mutual coupling of a sensor array [18]

$$\mathcal{L} = \frac{\|\mathbf{C} - \text{diag}(\mathbf{C})\|_F}{\|\mathbf{C}\|_F} \tag{18}$$

where $\|\cdot\|_F$ is the Frobenius norm, and $\left[\text{diag}(\mathbf{C})\right]_{i,j} = [\mathbf{C}]_{i,j}\, \delta_{i,j}$, where $[\mathbf{C}]_{i,j}$ it the (i, j)th entry of the matrix $\mathbf{C}$. Note that lower $\mathcal{L}$ is often preferred, to have lower degradation effect on DoA estimation algorithms.

E. 2D-DoA ESTIMATION ALGORITHMS

Many algorithms are used for 2D-DoA estimation with uniform or sparse planar arrays. For example, MUSIC, ESPRIT, PM, DoA matrix method (DMM) and others have been used with sparse arrays. This section gives a brief introduction to MUSIC with two variants and DMM.

1) MUSIC

MUSIC algorithm does not assume anything about the array geometry [67]. However, the maximum number of resolvable sources is limited by the number of physical sensors in the array, since it is required to find the noise subspace of the autocorrelation matrix. This algorithm is called direct-MUSIC, to distinguish it from other MUSIC variants discussed later in this section. For direct-MUSIC, if $\mathbf{x}(t)$ denotes the output of all N_t physical sensors, the covariance matrix is

$$\mathbf{R}_\mathbb{S} = \mathbb{E}\left[\mathbf{x}(t) \mathbf{x}^H(t) \right] \in \mathbb{C}^{N_t \times N_t} \tag{19}$$

where the subscript $\mathbb{S}$ denotes the set of physical array elements. The next steps are finding the eigenvalue decomposition and searching for the peaks in the pseudospectrum [22], [67], [91]

$$P_{\text{MUSIC}}(\theta, \phi) = \frac{1}{\mathbf{a}^H(\theta, \phi) \mathbf{E}_N \mathbf{E}_N^H \mathbf{a}(\theta, \phi)} \tag{20}$$

which means minimizing the distance from $\mathbf{a}(\theta_k, \phi_k)$ to the signal subspace. Note that $\mathbf{a}(\theta_k, \phi_k)$ in (20) does not depend on the data, and $\mathbf{E}_N \in \mathbb{C}^{N_t \times (N_t - K)}$ denotes the noise subspace. Again, $N_t > K$ is assumed.

2) DA-MUSIC AND SS-MUSIC

Direct augmentation MUSIC (DA-MUSIC) and spatial smoothing MUSIC (SS-MUSIC) are two MUSIC variants that utilize the coarray model of the physical array. Therefore, DA-MUSIC and SS-MUSIC can, in many cases, resolve more sources than the number of physical sensors. Both DA-MUSIC and SS-MUSIC start from the covariance matrix in (19) and vectorize it (i.e. stack columns one below the other) to yield

$$\mathbf{r} = \text{vec}(\mathbf{R}_\mathbb{S}) \tag{21}$$

Next, a new covariance matrix can be formed for each of DA-MUSIC and SS-MUSIC. Note that there are other possible ways to manipulate the vectorized covariance in (21) for use with DoA estimation algorithms (not necessarily MUSIC). For instance, correlating $\mathbf{r}$ with itself [53].

It is worth mentioning that *spatial smoothing* can be used to decorrelate correlated sources [92], or to exploit the difference coarray to achieve high DOF [14], [17], [60]. Many 2D-DoA estimation algorithms use it in the second regime, since this allows for resolving more sources than the number of sensors. However, spatial smoothing does not fully exploit all possible DOF.

3) DoA MATRIX METHOD

Yin *et al.* [93] proposed the DMM for two parallel linear arrays. Yin *et al.* [94] also explained the relation of their method to ESPRIT, and how ESPRIT can be considered a special case of the DoA matrix method. Later, Dai *et al.* [95] proposed an extended DMM (EDMM) which utilizes the sensors of both parallel linear arrays more effectively. This method first estimates the auto- and cross-correlations of both linear arrays, then performs eigenvalue decomposition to estimate the noise by averaging the $N_t - K$ smallest eigenvalues, then it forms the DoA matrix, which is used to get the azimuth and elevation estimates.

III. SPARSE ARRAY GEOMETRIES FOR 2D-DoA ESTIMATION

This section presents a comprehensive overview of the sparse array geometries employed for 2D-DoA estimation.

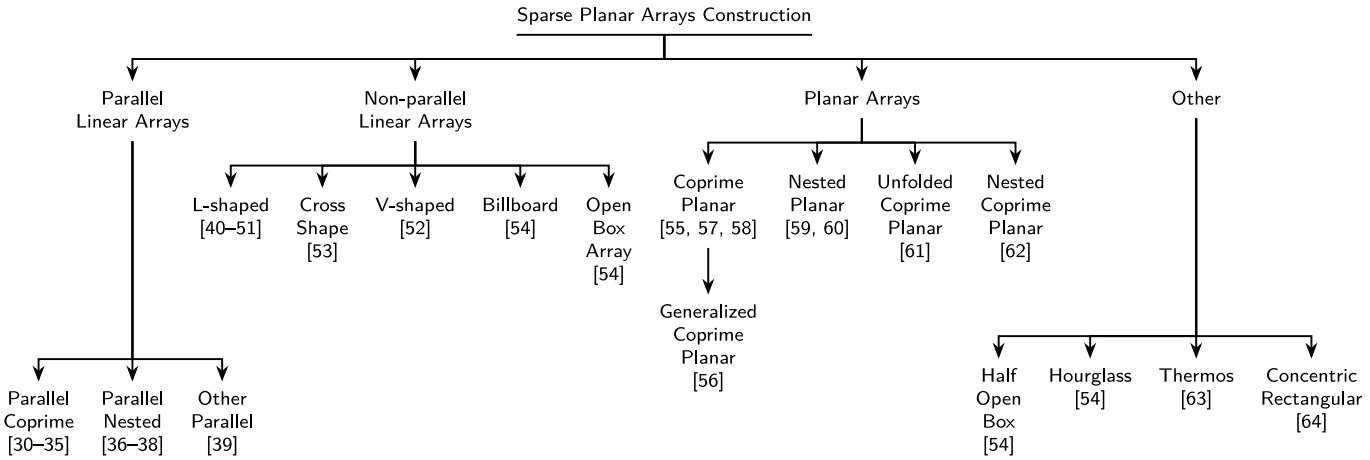

FIGURE 2. Classification of sparse 2D geometries based on the constituent arrays and the associated literature.

The geometries are classified, as shown in Fig. 2, into four broad categories: 1) arrays constructed using parallel linear arrays, 2) arrays constructed using non-parallel linear arrays, 3) arrays constructed using planar arrays, and 4) other geometries. In addition, a timeline of the usage of arrays from each category is shown in Fig. 3. Note that some papers may deal with more than one geometry such as the work of Liu and Vaidyanathan [54]. Another important note is that some of these geometries are named slightly differently by some authors. For instance, the parallel coprime array (PCA) is called coprime parallel array by two papers [31], [32], yet the rest of the authors use the name used in this work [30], [33]–[35]. This name also avoids confusing the PCA with the coprime planar array (CPA). The knowledge of sparse linear arrays, especially the *nested array* (NA) and the *coprime array* (CA) is important since many 2D sensor arrangements are constructed using a combination of these and possibly the *uniform linear array* (ULA).

This section describes the sensor arrays shown in Fig. 2 from left to right. The adopted classification categories based on the building blocks of the 2D array are:

1) Parallel linear arrays, which include PCA, parallel nested array (PNA), and other parallel structures. These are discussed in Section III-A.
2) Non-parallel linear arrays, which include various sparse L-shaped arrays, sparse cross-shaped array, sparse V-shaped arrays, billboard array, and open box array (OBA). These are discussed in Section III-B.
3) Planar arrays, which include CPA, generalized coprime planar array (GCPA), nested planar array (NPA), unfolded coprime planar array (UCPA), and nested coprime planar array (NCPA). These are discussed in Section III-C.
4) Other arrays, which include half open box array with two layers (HOBA-2), hourglass array, thermos array, and concentric rectangular array (CcRA). These are discussed in Section III-D.

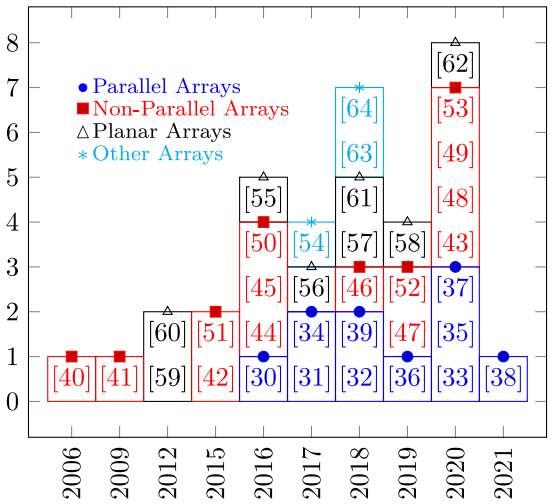

FIGURE 3. Timeline of papers using 2D sparse array geometries [30]–[64].

Since this work deals with *sparse* array geometries, it is useful to mention that the term *sparse* can have different appearances in the context of DoA estimation:

1) Sparse sensor array: where sensors are placed on *some* intersections of a uniform grid. This is equivalent to having *some* sensors with inter-element spacing of unity and the rest greater than unity (assuming a normalized fundamental inter-sensor spacing d). Put another way: the inter-element spacing is a positive integer (normalized). Another name that is sometimes used for this meaning is *thinned array*. This meaning is used throughout this manuscript.
2) Uniform sparse sensor array: where the spacing of all sensor elements are *identical* and greater than unity. This is a special case of the previous one, and essentially the resultant array is a uniform array. In case of linear arrays, that resultant array is referred to as *sparse ULA*, some examples of this usage are [96], [97].

3) Sparse recovery: a method from the compressive sensing framework used in some DoA estimation algorithms.

The next subsection starts with parallel arrays as building blocks for 2D arrays. Then, non-parallel, planar, and other arrays follow.

A. PARALLEL ARRAYS

This section describes 2D arrays made of two, or more, parallel arrays. In particular, the parallel coprime array (PCA), the three parallel coprime array (TPCA), and the parallel nested array (PNA) are considered. In addition, other reported parallel arrays that does not fall under any of these categories are also mentioned. Note that 2D arrays made of two parallel ULAs are not considered in this survey.

1) PARALLEL COPRIME ARRAY (PCA)

This section presents an overview of parallel coprime array (PCA) geometry [30]–[33]. The structure of PCA is shown in Fig. 4a, where two uniform linear arrays (ULAs) are in parallel (spaced by d_x). One of them has M_1 elements with $M_2 d_y$ inter-element spacing (shown in blue boxes), and the other has M_2 elements with $M_1 d_y$ inter-element spacing (shown in black circles). In this geometry, M_1 and M_2 are coprime integers, and the example of Fig. 4a assumes $M_1 = 3$ and $M_2 = 4$. Note that often $M_1 < M_2$ is assumed without loss of generality. The set of array elements is [32]

$$\mathbb{S} = \{(0, mM_2 d_y) | 0 \le m \le M_1 - 1\} \cup \{(d_x, nM_1 d_y) | 0 \le n \le M_2 - 1\}. \quad (22)$$

The work in [33] finds the cross covariance between the two arrays as a first step in estimating 2D-DoA, then decouples the angles α_k and β_k, finds α_k using least spectral search (1D-MUSIC over each subarray), and presents a least squares solution for automatic pairing of β_k. A variant of PCA using two symmetric parallel coprime arrays was also reported [31].

2) THREE PARALLEL COPRIME ARRAY (TPCA)

This section presents an extension to the PCA of the previous section using a third parallel linear array (LA) [34], [35]. A modified version of the PCA is the three parallel coprime structure presented in [35], where the third LA starts after the end of the other two LAs as shown in Fig. 4b, where the first ULA has M_2 elements with inter-element spacing $M_1 d_y$ (shown in blue boxes) and the other two ULAs have inter-element spacing $M_2 d_y$ (shown in black circles). The example shown in Fig. 4b assumes $M_1 = 3$, $M_2 = 4$, and $L = 3$. In addition, the second ULA is spaced by d_x from the y-axis and has M_1 elements, whereas the third ULA is spaced by Ld_x, $L > d_x$ from the second ULA and has M_1 elements. The set of elements is [35]

$$\begin{aligned}\mathbb{S} = {} & \{(0, mM_1 d_y) | 0 \le m \le M_2 - 1\} \\ & \cup \{(d_x, nM_2 d_y) | 1 \le n \le M_1 - 1\} \\ & \cup \{(Ld_x + d_x, pM_2 d_y + M_1 M_2 d_y) | 0 \le p \le M_1 - 1\}. \quad (23)\end{aligned}$$

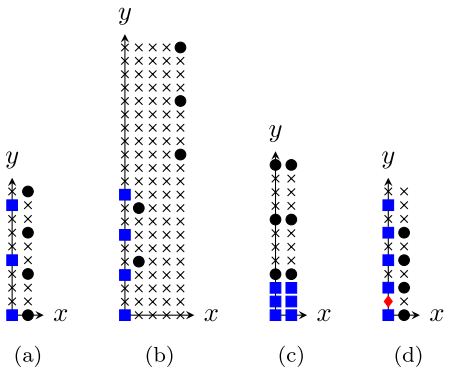

FIGURE 4. Examples of 2D sparse arrays constructing using parallel linear arrays. (a) PCA. (b) Three parallel coprime array. (c) PNA. (d) Two parallel sparse ULAs with extra sensor (shown by a red diamond).

Another work presented three parallel coprime array where an extra LA can be added on the negative x-axis of the PCA in (22) to form the three parallel coprime array [34]. The middle array has $2M_1$ elements with inter-element spacing of $M_2 d_y$, and the outer coprime LAs has M_2 elements with inter-element spacing of $M_1 d_y$, where $d_y \le \lambda/2$, M_1 and M_2 are coprime integers with $M_1 < M_2$. In addition, the LAs are spaced by $d_x \le \lambda/2$.

3) PARALLEL NESTED ARRAY (PNA)

Parallel nested arrays (PNAs) were reported in [36]–[38]. All three papers utilized two identical parallel nested linear arrays (NLAs) [17] (shown in Fig. 4c with $N_1 = N_2 = 3$). Assuming each linear array has N elements, the total number of elements is $2N$. The set of antenna elements is

$$\mathbb{S} = \{(0, md_y) | m \in \mathfrak{g}\} \cup \{(d_x, md_y) | m \in \mathfrak{g}\}, \mathfrak{g} = \{0, 1, \ldots, N_1 - 1, N_1, 2(N_1 + 1) - 1, \ldots, N_2(N_1 + 1) - 1\} \quad (24)$$

Li et al. [36] utilized a DMM (see Section II-E3) which allows getting paired estimates for u_k and v_k. He et al. [38] proposed an algorithm using FOC for enhancing the DOF, and reported a maximum DOF of $6N_2(N_1 + 1) - 3$.

4) OTHER PARALLEL ARRAYS

Other than the PCA or the PNA, Zheng et al. [39] proposed two parallel ULAs with an extra sensor. The two ULAs are spaced by $\lambda/2$, and each of the two ULAs has inter-sensor spacing of λ, and the extra sensor is placed at $\lambda/2$ from the start of the first ULA, as shown in Fig. 4d, where the first ULA (denoted subarray Y) has $N + 1$ elements and is represented by blue squares, the extra sensor by a red square, and the second ULA (denoted subarray Z) has N elements and is represented by black circles. The first linear array that is made up of subarray Y and the extra sensor is denoted Subarray X. Therefore, the set of array elements can be written as

$$\mathbb{S} = \{(0, 2md_y) | 0 \le m \le N\} \cup \{(0, d_y)\} \cup \{(d_x, 2nd_y) | 0 \le n \le N - 1\}. \quad (25)$$

where $d_y = d_x = \lambda/2$.

Zheng et al. [39] proposed this array assuming the number of sources is less than the number of elements in subarray Z. They estimate a propagator matrix, which yields estimates of u_k and v_k. An important step in the algorithm is to exclude the ambiguous estimates of u_k which relies on the fact that the unambiguous u_k will be orthogonal to the noise subspace of subarray X.

B. NON-PARALLEL ARRAYS

This section describes 2D arrays made of non-parallel linear arrays, namely: the L-shaped, cross-shaped, and V-shaped arrays. In addition, the billboard array and open box array (OBA) are also mentioned for a more complete big picture.

1) L-SHAPED ARRAY

The L-shaped array is arguably the most straightforward extension from 1D to 2D arrays, since it requires two orthogonal ULAs. Many works were published utilizing this structure like Hua et al. [98] and Liang and Liu [66]. However, the focus here is on works utilizing orthogonal sparse linear arrays like [40]–[51]. It can be argued that the L-shaped array is sparse when compared to the URA, but since it is composed of ULAs, they can be treated as non-sparse in this survey. Note that many works on L-shaped and cross-shaped arrays use the x-z plane for the placement of the sensor array, and this is hinted by showing an example in Fig. 5a.

One approach of constructing sparse L-shaped arrays [44], [45] (shown in Fig. 5a) used two orthogonal two-level nested arrays [17] along the x- and z-axes. As shown in Fig. 5a, the first (dense) ULA of each nested array has inter-element spacing $d_1 = d_x = d_y$ and the other ULA has the wider $d_2 = (N_1 + 1)d_1$ inter-element spacing. Dong et al. [44] used signal subspace joint diagonalization (SSJD) for automatic pairing of azimuth and elevation angles.

Another approach uses a ULA along the x-axis with inter-element spacing $d_x = \lambda/2$, and a simple sparse linear array along the z-axis made up of a ULA with $d_z = \lambda$ with an extra sensor at a distance $\lambda/2$ from the origin [50]. After computing the cross correlation between the two subarrays (along the x- and z-axes), the ambiguous elevation estimates are obtained. Next, the ambiguity is removed, then the estimated elevation angles are utilized to estimate the azimuth [50].

Another work utilized sparse LAs along each axis. Each sparse LA is made up of two interleaved ULAs [49], and the largest contiguous ULA in the difference coarray is used for estimation. The estimation of azimuth and elevation are done separately using MUSIC, and cross covariance is used to pair the azimuth and elevation estimates. Coprime arrays were also utilized in the legs of the L-shaped array [42], [43]. For instance, the work by Elbir [43] showed the possibility of resolving M_1M_2 sources while having $2M_1 + M_2 - 1$ sensors in each leg. According to Elbir [43], this requirement of $4M_1 + 2M_2 - 3$ sensors is less than CPA and GCPA which are discussed in Section III-C1.

2) CROSS-SHAPED ARRAY

Wu and Zhu [53] considered a uniform cross array, and a sparse symmetric cross array for the estimation of three parameters: azimuth, elevation, and range of a single source in the near-field or far-field. For the uniform cross array, two orthogonal ULAs are used with $N_x := 2M_x + 1$ and $N_y := 2M_y + 1$ elements on the x- and y-axes, respectively. The set of array elements can be written as

$$\mathbb{S} = \{(md, 0)| - M_x \leq m \leq M_x\} \cup \{(0, nd)| - M_y \leq n \leq M_y\}, \quad (26)$$

where d is the fundamental spacing. To construct the sparse symmetric cross array, each ULA is replaced by a symmetric sparse linear array. In this case, the set of elements becomes

$$\mathbb{S} = \{(md, 0)|m \in \mathbb{G}_x\} \cup \{(0, nd)|n \in \mathbb{G}_y\}, \quad (27)$$

where $\mathbb{G}_x$ is a symmetric set (about the origin) and is a subset of $\{-M_x, -M_x+1, \ldots, -1, 0, 1, \ldots, M_x-1, M_x\}$ and $\mathbb{G}_y$ is a subset of $\{-M_y, -M_y+1, \ldots, -1, 0, 1, \ldots, M_y-1, M_y\}$. An example of this structure when $M_x = M_y = 3$ and $\mathbb{G}_x = \mathbb{G}_y = \{-3, -2, 0, 2, 3\}$ is shown in Fig. 5b where blue boxes resemble $\mathbb{G}_x$ and black circles resemble $\mathbb{G}_y$. Note that the two linear arrays share a common element at the origin, the blue boxes denote the first linear array, the black circles denote the second linear array, and the crosses denote empty locations.

The algorithm proposed by Wu and Zhu [53] has two main steps. The first step is finding the 2D-DoA by computing the cross correlation matrix, vectorizing it, and correlating the resultant vectors. The authors chose to apply atomic norm minimization to get the angle estimates, and justified why this is better than some other methods like 2D-MUSIC, and the fact that they avoided the grid mismatch issue. They further mentioned why their method can work for sparse linear arrays without spatial smoothing which causes aperture loss as was done in oblique projection (OP)-MUSIC [99]. While this suffices for 2D-DoA estimation in the far-field, the authors also described the second step for the near-field case, which is estimating the range.

3) V-SHAPED ARRAY

A generalization to the L-shaped array is the V-shaped array, where the ninety-degrees angle between the two LAs of the L-shaped array becomes $\Omega < 90$ deg. Elbir [52] proposed V-shaped coprime array (VCA) and V-shaped nested array (VNA). An example of VCA is shown in Fig. 5c with $M_1 = 2$, $M_2 = 5$, and $\Omega = 53.28$ deg. The value of Ω is selected such that the estimation of azimuth and elevation is uncoupled [52]. The author reports that the V-shaped array can resolve the same number of sources with less number of sensors when compared to CPA or GCPA (discussed in Section III-C1).

4) BILLBOARD ARRAY

The billboard array is constructed using an L-shaped array with an extra linear array at 45 degrees from both legs of the

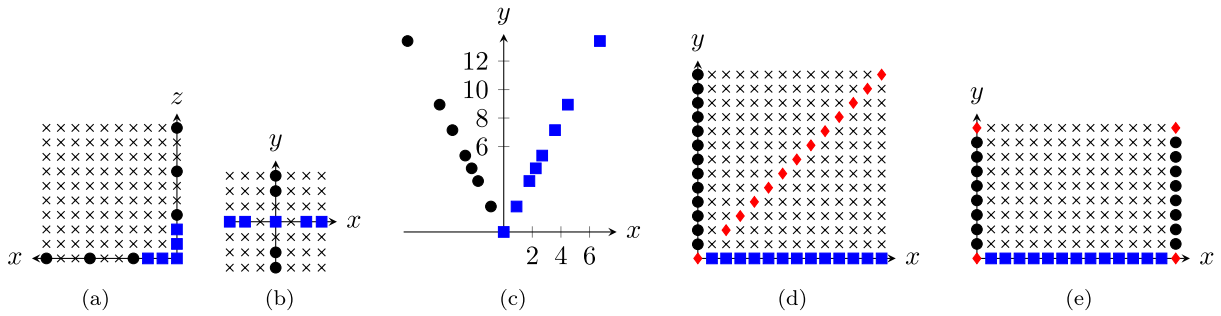

FIGURE 5. Examples of 2D sparse arrays constructed using non-parallel linear arrays. (a) L-shaped sparse array using two ULAs with an extra sensor. (b) Cross-shaped sparse array. (c) V-shaped coprime array. (d) Billboard array. (e) Open box array (OBA).

L-shaped array. An example of such array is shown in Fig. 5d. This array enjoys a hole-free difference coarray [54].

5) OPEN BOX ARRAY

The open box array (OBA) is also formed using three LAs, orthogonal to each other, which are the three edges of rectangle. The OBA can also be considered as two L-shaped arrays sharing a LA. An example OBA when $N_x = 15$ and $N_y = 10$ is shown in Fig. 5e where blue boxes represent $\mathbb{G}$, black circles represent $\mathbb{H}_1$ and $\mathbb{H}_2$, and red diamonds represent $\mathbb{F}$. For two integers N_x and N_y, the set of sensor locations for the OBA can be written as [54]

$$\mathbb{S} = \mathbb{G}_1 \cup \mathbb{H}_1 \cup \mathbb{H}_2 \cup \mathbb{F} \tag{28}$$

where

$$\mathbb{G}_1 = \{(l_x, 0)|l_x \in \mathfrak{g}_1\}, \mathfrak{g}_1 = \{1, 2, \ldots, N_x - 2\} \tag{29}$$
$$\mathbb{H}_1 = \{(0, l_y)|l_y \in \mathfrak{h}_1\}, \mathfrak{h}_1 = \{1, 2, \ldots, N_y - 2\} \tag{30}$$
$$\mathbb{H}_2 = \{(N_x - 1, l_y)|l_y \in \mathfrak{h}_2\}, \mathfrak{h}_2 = \{1, 2, \ldots, N_y - 2\} \tag{31}$$
$$\mathbb{F} = \{(0, 0), (N_x - 1, 0), (0, N_y - 1), (N_x - 1, N_y - 1)\} \tag{32}$$

The difference coarray is given by

$$\mathbb{D} = \{(m_x, m_y) \in \mathbb{Z}^2| \\ -N_x + 1 \leq m_x \leq N_x - 1, -N_y + 1 \leq m_y \leq N_y - 1\} \tag{33}$$

which is a uniform rectangular array. Generalizations of OBA are discussed in Section III-D1. In particular, the generalizations will ensure the same continuous difference coarray in (33) while increasing inter-sensor spacing, thus reducing mutual coupling effects.

The two arrays (billboard, and OBA) are constructed using ULAs, and the performance of both is generally exceeded by three newly-developed arrays which are: HOBA-2 [54], the hourglass array [54], and the thermos array [63], discussed in Sections III-D1, III-D2, and III-D3, respectively. Therefore, billboard and OBAs are not discussed further.

C. PLANAR ARRAYS

This section describes 2D arrays made by interleaving two planar arrays like the coprime planar array (CPA), and the unfolded coprime planar array (UCPA). In addition, other planar structures like the nested planar array (NPA) or the nested coprime planar array (NCPA) are examined.

1) COPRIME PLANAR ARRAY (CPA)

Coprime planar array (CPA) results from interleaving two uniform planar arrays, which results from interleaving two uniform planar arrays, which are denoted as subarrays. The CPA [55], [57], [58] is described first. Then, the general way of interleaving the subarrays, the generalized oprime planar array (GCPA) [56] is described. The latter is just a generalization of the former where the number of elements along the x- and y-axes need not be equal. Next, some details of 2D-DoA estimation algorithms using these arrays are outlined.

A CPA is constructed using two interleaved uniform square arrays. Denoting each uniform square array as a subarray, there are $M_1 \times M_1$ and $M_2 \times M_2$ elements in subarrays 1 and 2, respectively. Since the two subarrays share a common element at the origin, the total number of elements is $M_1^2 + M_2^2 - 1$. The set of antenna elements is [55], [57], [58]

$$\mathbb{S} = \{(md_1, nd_1)|0 \leq m, n \leq M_1 - 1\} \\ \cup\{(pd_2, qd_2)|0 \leq p, q \leq M_2 - 1\} \tag{34}$$

where $d_1 = M_2 d$, $d_2 = M_1 d$, $d = \lambda/2$, and m, n, p, q are integers.

The GCPA structure, proposed by Zheng *et al.* [56], has more DOF and yields better DoA estimates for the same number of sensors as CPA. GCPA relaxes the condition of using uniform square subarrays, and allows uniform rectangular subarrays. An example of GCPA is shown in Fig. 6a. GCPA is made up using two interleaved URAs having the dimensions of $M_1 \times N_1$ and $M_2 \times N_2$ whereas CPA is constructed from two interleaved uniform square arrays. Here, M_1 (M_2) is the number of elements of the first (second) URA along the x-axis, N_1 (N_2) is the number of elements of the first (second) URA along the y-axis, and $N_1 = M_1$, $N_2 = M_2$ in the case of restricting URAs to become uniform square arrays. In the

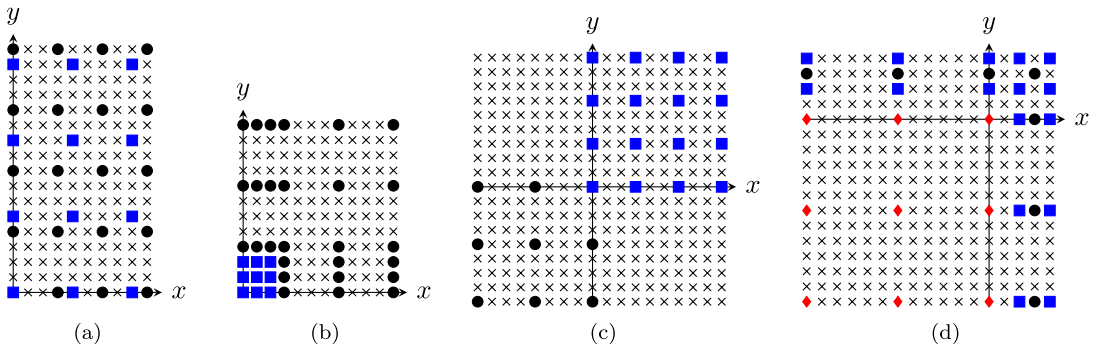

FIGURE 6. Examples of sparse arrays constructed using planar subarrays. Blue squares represent subarray 1. Black circles represent subarray 2. Red diamonds represent common elements. (a) Generalized coprime planar array (GCPA); CPA is a special case. (b) Nested planar array (NPA). (c) Unfolded coprime planar array (UCPA). (d) Nested coprime planar array (NCPA).

case of GCPA, the set of array elements becomes

$$\mathbb{S} = \{(mM_2d_x, n\,N_2d_y)|0 \le m \le M_1 - 1, 0 \le n \le N_1 - 1\} \cup \{(pM_1d_x, q\,N_1d_y)|0 \le p \le M_2 - 1, 0 \le q \le N_2 - 1\} \quad (35)$$

where d_x (d_y) is the fundamental distance along the x- (y-) axis, and is often chosen to be $\lambda/2$.

Algorithms for arbitrary arrays do not utilize the uniform nature of subarrays, and they tend to be more complex than specially tailored algorithms. Therefore, a special efficient method for CPAs was developed that utilizes uniformity of subarrays [55]. The proposed method essentially limits the 2D-MUSIC search requirement to a small subset; hence, the method is named the partial spectral search (PSS). The first two steps are to estimate the covariance matrix of each subarray, and detail how to choose an arbitrary small sector to find some ambiguous peaks, which they prove to be related to ambiguous peaks in other sectors. To pick the true peaks, defining the difference between the two subarrays allows for selecting the K values closest to the true peaks which yield the estimate $(\hat{u}_k, \hat{v}_k)$ and consequently $(\hat{\phi}_k, \hat{\theta}_k)$.

Another work utilized the signal subspace in addition to the noise subspace to avoid any spectral search [57]; rather, a double polynomial rooting algorithm is utilized. Furthermore, a study on the separation of coherent and uncorrelated signals was reported [58], where unitary ESPRIT is used for the planar geometry and root-MUSIC for a linear coprime array.

2) NESTED PLANAR ARRAY (NPA)

The nested planar array (NPA) was proposed by Pal and Vaidyanathan [59], [60] as an extension to the 1D nested array, and it can provide $\mathcal{O}(MN)$ virtual sensors continuously in the difference coarray while only having $\mathcal{O}(M + N)$ sensors. Here M denotes the number of sensors in a dense grid, and N is the physical sensors in a sparse grid. For instance, using two linear nested arrays with $N_1 = N_2 = 3$, the nested planar array looks like Fig. 6b, where N_1 is the number of elements in the dense LA, and N_2 is the number of elements in the sparse LA. The authors also show that with effective selection of M and N, $\mathcal{O}(N_t^2)$ sources can be identified using the difference coarray. To achieve that, they explain how to build a covariance-like matrix of dimensions $\mathcal{O}(N_t^2)\times\mathcal{O}(N_t^2)$, which corresponds to virtual sensors, from only the estimated covariance matrix of size $N_t \times N_t$.

3) UNFOLDED COPRIME PLANAR ARRAY (UCPA)

Instead of interleaving two uniform square arrays (subarrays) to construct the CPA in Section III-C1, one of the uniform square arrays is *unfolded*, that is, flipped across the x-axis or the y-axis. Therefore, the two subarrays lie in different quadrants. Fixing one subarray at the first quadrant, Zheng *et al.* [61] investigated the performance of 2D-DoA estimation when the other subarray is in the three other quadrants. They also proposed an ambiguity-free MUSIC algorithm, and further utilized a successive method of implementing it to relief the computational burden. They concluded that when one subarray is flipped across the line $y = -x$ (so it lies in the third quadrant), the performance is better than other flipped structures and the traditional CPA. Fig. 6c shows this case where the first (second) subarray has $M_1 \times M_1$ ($M_2 \times M_2$) sensor elements, and the set of array elements is

$$\mathbb{S} = \{(md_1, nd_1)|0 \le m, n \le M_1 - 1\} \cup \{(pd_2, qd_2)| - (M_2 - 1) \le p, q \le 0\} \quad (36)$$

where $d_1 = M_2d$, $d_2 = M_1d$, and $d = \lambda/2$.

4) NESTED COPRIME PLANAR ARRAY (NCPA)

The structure of nested coprime planar array (NCPA) is quite involved to describe, despite being simple in design. Among the motivations reported by Si et al. [62] is that their NCPA can outperform all other CPAs, namely GCPA [56], CPA [55], [57], [58], and UCPA [61] in terms of being able to detect more sources than the number of sensor elements. The NCPA also produces two virtual coprime planar arrays that are used to obtain two sets of DoA estimation that are linked together to get the unique directions of arrival. Note that Si *et al.* [62] did not use the *NCPA* term.

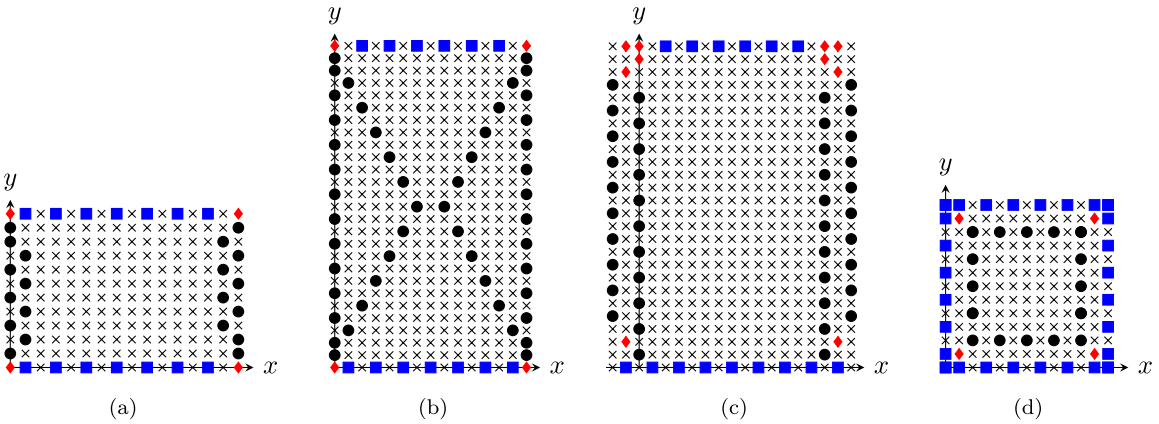

FIGURE 7. Additional examples of 2D sparse arrays. (a) Half open box array with two layers (HOBA-2). (b) Hourglass array. (c) Thermos array. (d) Concentric rectangular array.

The NCPA is constructed from two sparse planar arrays, unlike the other types: GCPA, CPA, and UCPA which are constructed from uniform planar arrays. Each sparse planar array is made up of a nested planar array (NPA). Each NPA is composed of a dense subarray and a sparse subarray. The example of this structure is shown in Fig. 6d. In this example, $M_1 = 2$, and $M_2 = L = 3$. The NPA is constructed from the elements of two orthogonal nested linear arrays (NLAs) and the elements at the intersections of lines, in the first quadrant, emerging from each sensor element and orthogonal to the nested linear array. Mathematically, the set of array elements is

$$\mathbb{S} = \{(m, n)|m, n \in \mathbb{S}_{\text{NPA1}}\} \cup \{(m, n)|m, n \in \mathbb{S}_{\text{NPA2}}\}. \quad (37)$$

This equation just describes the fact that the subarrays of the NCPA are made up of NPAs. Now the NPAs are made up of two orthogonal NLAs and other sensors, all of them are described by

$$\begin{aligned}\mathbb{S}_{\text{NPA1}} &= \{-L+1, -L+2, \ldots, 0\} \times M_1 M_2 d \\ &\quad \cup \{0, 1, \ldots, M_1 - 1\} \times M_2 d, \quad (38)\\ \mathbb{S}_{\text{NPA2}} &= \{-L+1, -L+2, \ldots, 0\} \times M_1 M_2 d \\ &\quad \cup \{0, 1, \ldots, M_2 - 1\} \times M_1 d, \quad (39)\end{aligned}$$

where M_1, M_2 are coprime positive integers, and L is an integer.

D. OTHER 2D ARRAYS

This section describes four more 2D sparse arrays that does not readily fall under any of the previous three categories. In particular, the half open box array with two layers (HOBA-2), the hourglass array, the thermos array, and the concentric rectangular array (CcRA) are considered.

1) HALF OPEN BOX ARRAY-2 (HOBA-2)

The half open box array with two layers (HOBA-2) is an extension of the half open box array (HOBA) which is a special case of the partial open box array (POBA). The partial open box array (POBA) is a systematic redistribution of elements in the OBA (Section III-B5) to reduce closely-spaced elements which reduces mutual coupling. An example of this array with $N_x = 16$ and $N_y = 12$ is shown in Fig. 7a, where black circles stand for $\mathbb{H}_1, \mathbb{H}_2$, blue squares stand for $\mathbb{G}_1, \mathbb{G}_2$, and red diamonds stand for $\mathbb{F}$. If some elements of $\mathbb{G}_1$ of the OBA (28) are redistributed on the opposite (empty) side of the OBA, the elements of POBA can be written as [54]

$$\mathbb{S} = \mathbb{G}_1 \cup \mathbb{G}_2 \cup \mathbb{H}_1 \cup \mathbb{H}_2 \cup \mathbb{F} \quad (40)$$

where

$$\mathbb{G}_1 = \{(\ell_x, 0)|\ell_x \in \mathfrak{g}_1\}, \quad \mathfrak{g}_1 = \{1, 2, \ldots, N_x - 2\} \quad (41)$$

$$\mathbb{G}_2 = \{(\ell_x, N_y - 1)|\ell_x \in \mathfrak{g}_2\}, \ \mathfrak{g}_2 = \{1, 2, \ldots, N_x - 2\} \quad (42)$$

where $\mathfrak{g}_1$ and $\mathfrak{g}_2$ are subsets of $\{1, 2, \ldots, N_x - 2\}$ with $|\mathfrak{g}_1| + |\mathfrak{g}_2| = N_x - 2$. Note that POBA is still defined using N_x and N_y as the OBA, and $\mathbb{H}_1, \mathbb{H}_2$, and $\mathbb{F}$ are as defined in (30), (31), and (32), respectively.

If $\mathfrak{g}_1$ and $\mathfrak{g}_2$ are chosen to be of the following form, the array is called half open box array (HOBA)

$$\mathfrak{g}_1 = \{1 + 2\ell \mid 0 \le \ell \le \lfloor (N_x - 3)/2 \rfloor\}, \quad (43)$$

$$\mathfrak{g}_2 = \{N_x - 1 - 2\ell \mid 1 \le \ell \le \lfloor (N_x - 2)/2 \rfloor\}. \quad (44)$$

Similar argument can be applied to the other ULAs (on the right and left) of the OBA, which results in the partial open box array with L levels (POBA-L)

$$\mathbb{S} = \mathbb{G}_1 \cup \mathbb{G}_2 \cup \left(\bigcup_{\ell=1}^{L} \mathbb{H}_{1,\ell} \cup \mathbb{H}_{2,\ell} \right) \cup \mathbb{F} \quad (45)$$

where each of $\mathfrak{g}_1$ and $\mathfrak{g}_2$ is a partition of $\{1, 2, \ldots, N_x - 2\}$, $\{\mathfrak{h}_{1,\ell}\}_{\ell=1}^{L}$ is a partition of $\{1, 2, \ldots, N_y - 2\}$, and $\mathfrak{h}_{2,\ell} = N_y - 1 - \mathfrak{h}_{1,\ell}$ for $\ell = 1, \ldots, L$. Note that a third positive integer $L \le N_x/2$ is required to design partial open box array with L levels (POBA-L). If L is chosen to be 2, $\mathfrak{g}_1$ and $\mathfrak{g}_2$ as in (43), (44), and

$$\mathfrak{h}_{1,1} = \{1 + 2\ell \mid 0 \le \ell \le \lfloor (N_y - 3)/2 \rfloor\} \cup \{N_y - 2\}, \quad (46)$$

$$\mathfrak{h}_{1,2} = \{2\ell \mid 1 \le \ell \le \lfloor (N_y - 3)/2 \rfloor\}, \quad (47)$$

the array is called half open box array with two layers (HOBA-2). The next subsection describes the hourglass array, which is a POBA-L array.

2) HOURGLASS ARRAY

Hourglass array is a special case of POBA, which was presented by Liu and Vaidyanathan [54]. The virtues of hourglass arrays include 1) having the same coarray as the OBA (using the same aperture), 2) having a hole-free difference coarray (based on the previous virtue), and 3) reduced mutual coupling compared with the OBA. Following the notation in Section III-D1, and for positive integers N_x and N_y, and L layers, the element locations of the array can be described by

$$\mathfrak{g}_1 = \{1 + 2\,p \mid 0 \le p \le \lfloor (N_x - 3)/2 \rfloor\}, \tag{48}$$

$$\mathfrak{g}_2 = \{N_x - 1 - 2p \mid 1 \le p \le \lfloor (N_x - 2)/2 \rfloor\}. \tag{49}$$

and $\mathfrak{h}_{1,\ell}$ as in (50), as shown at the bottom of the page, where

$$L = \begin{cases} \lfloor (N_y + 1)/4 \rfloor, & \text{if } N_y \text{ is odd,} \\ \lfloor N_y/8 + 1 \rfloor, & \text{if } N_y \text{ is even.} \end{cases} \tag{51}$$

An example for hourglass array is shown in Fig. 7b with $N_x = 15$ and $N_y = 27$.

To demonstrate the robustness of HOBA-2 and hourglass arrays in presence of mutual coupling, the authors compared the arrays with billboard, OBA, and URA using 2D unitary ESPRIT without modifications to account for mutual coupling. It was shown that hourglass performs best compared to other arrays, especially with low snapshots [54].

3) THERMOS ARRAY

Sun *et al.* [63] proposed the thermos array as an improvement to the hourglass array in terms of reducing mutual coupling. Since the elements with vertical inter-element spacing of d were about five times larger than the horizontal ones, they proposed the thermos array which reduces these vertical spacings. Two parameters are enough to design a thermos array: $N_x \in \mathbb{Z}^+$ and $N_y \in \mathbb{Z}^+$ which yield the total number of sensors as $N_x + 2\,N_y - 2$. An example of a thermos array is shown in Fig. 7c with $N_x = 15$ and $N_y = 27$. In Fig. 7c, black circles represent $\mathbb{S}_1, \mathbb{S}_2, \mathbb{R}_1, \mathbb{R}_2$, blue boxes represent $\mathbb{B}$, $\mathbb{T}$, and red diamonds represent $\mathbb{F}$. The thermos array has a rectangular shape and is designed using six ULAs with inter-sensor spacing of $2d$ plus four or ten more elements at the corners depending on the number of elements in the y direction, N_y. If N_y is even, ten elements are needed, and four if N_y is odd. The set of array elements $\mathbb{S}$ can be written as a union of a top, bottom, two left, and two right ULAs plus the extra sensors at the corner denoted by $\mathbb{F}$. Thus,

$$\mathbb{S} = \mathbb{B} \cup \mathbb{T} \cup \mathbb{S}_1 \cup \mathbb{S}_2 \cup \mathbb{R}_1 \cup \mathbb{R}_2 \cup \mathbb{F} \tag{52}$$

where

$$\mathbb{B} = \{(-1 + 2\ell, 0) | 0 \le \ell \le (N_x + N_x \text{mod} 2)/2\} \tag{53}$$

$$\mathbb{T} = \{(2\ell + 1 + N_x \text{mod} 2, N_y - 2) | \; 0 \le \ell \le (N_x - N_x \text{mod} 2)/2 - 2\} \tag{54}$$

$$\mathbb{S}_1 = \{(-2, 2\ell) | 1 \le \ell \le (N_y - N_y \text{mod} 2)/2 - 2\} \tag{55}$$

$$\mathbb{S}_2 = \{(0, 1 + 2\ell) | \; 1 \le \ell \le (N_y - N_y \text{mod} 2)/2 - 1 - N_y \text{mod} 2\} \tag{56}$$

$$\mathbb{R}_1 = \{(N_x - 1, -1 + 2\ell) | \; 1 \le \ell \le (N_y - N_y \text{mod} 2)/2 - 1 - N_y \text{mod} 2\} \tag{57}$$

$$\mathbb{R}_2 = \{(N_x + 1, 2\ell) | 1 \le \ell \le (N_y - N_y \text{mod} 2)/2 - 2\} \tag{58}$$

and

$$\mathbb{F} = \{(-1, N_y - 2), (0, N_y - 2), (N_x - 1, N_y - 2), (N_x, N_y - 2)\} \tag{59}$$

when N_y is even, or

$$\mathbb{F} = \{(-1, N_y - 2), (0, N_y - 2), (N_x - 1, N_y - 2), (N_x, N_y - 2), (-1, 2), (N_x, 2), (-1, N_y - 4), (0, N_y - 3), (N_x - 1, N_y - 3), (N_x, N_y - 4)\} \tag{60}$$

when N_y is odd. Note that $N_x \text{mod} 2 = 0$ if N_x is even, and $N_x \text{mod} 2 = 1$ if N_x is odd.

4) CONCENTRIC RECTANGULAR ARRAY (CcRA)

Rajamäki and Koivunen [64] proposed the CcRA which can be thought of as a modification of the boundary array. An example of the CcRA is shown in Fig. 7d with $N_x = N_y = 12$, blue squares for $\mathbb{G}_o$, and black circles for $\mathbb{G}_i$. The total number of sensors is $2(N_x + N_y)$. Although the paper does not directly implement this array for 2D-DoA estimation, it is cited as it proposes a sparse 2D array. In general, for even $N_x, N_y \ge 2$, the CcRA is given by

$$\mathbb{S} = \mathbb{G}_o \cup \mathbb{G}_m \cup \mathbb{G}_i$$

where

$$\mathbb{G}_o = \{(p_x, p_y) | p_x \in \mathbb{P}_0(N_x), p_y \in \{0, N_y\}\} \cup \{(p_x, p_y) | p_x \in \{0, N_x\}, p_y \in \mathbb{P}_0(N_y)\} \tag{61}$$

$$\mathbb{G}_m = \{(p_x, p_y) | p_x \in \mathbb{P}_1(N_x), p_y \in \{1, N_y - 1\}\} \cup \{(p_x, p_y) | p_x \in \{1, N_x - 1\}, p_y \in \mathbb{P}_1(N_y)\} \tag{62}$$

$$\mathbb{G}_i = \{(p_x, p_y) | p_x \in \mathbb{P}_2(N_x), p_y \in \{2, N_y - 2\}\} \cup \{(p_x, p_y) | p_x \in \{2, N_x - 2\}, p_y \in \mathbb{P}_2(N_y)\} \tag{63}$$

and

$$\mathbb{P}_0(N) = \{0, N\} \cup \{1 : 2 : N - 1\}$$

$$\mathbb{P}_1(N) = \{0, 1, N - 1, N\}$$

$$\mathbb{P}_2(N) = \{2 : 2 : N - 2\}$$

$$\mathfrak{h}_{1,\ell} = \begin{cases} \{2p,\ N_y - 1 - 2p \mid 1 \le p \le \lfloor (N_y - 1)/4 \rfloor\} \cup \{1,\ N_y - 2\}, & \text{if } \ell = 1, \\ \{2\ell - 1,\ N_y - 2\ell\}, & \text{if } N_y \text{ is odd and } 0 \le \ell \le L, \\ \{2\ell - 1,\ 2\lfloor N_y/4 \rfloor - 2\ell + 3,\ 2\lceil N_y/4 \rceil + 2\ell - 4,\ N_y - 2\ell\}, & \text{if } N_y \text{ is even and } 2 \le \ell \le L, \end{cases} \tag{50}$$

TABLE 2. Comparison between physical sensors and achievable degrees of freedom for sparse array geometries.

Array		Ref.	Number of Sensors, N_t	Max DOF
Parallel	Coprime	[30]	$2M_1 + M_2$	$(4M_1^2 + 4M_1M_2 + M_2^2 - 1)/8$
		[31]	$4M_1 + 2M_2 - 2$	$4M_1M_2 - 1$
		[32]	$M_1 + M_2$	$\mathcal{O}\left((M_1 + M_2)^2\right)$
		[33]	$M_1 + M_2$	-
		[34]	$2M_1 + 2M_2$	$2M_1 + 2M_1M_2 - 1$
		[35]	$2M_1 + M_2 - 1$	$\lfloor (4M_1^2 + 4M_1M_2 + M_2^2 - 1)/8 \rfloor$
	Nested	[36]	$2N,\ N := N_1 + N_2$	$N_2(N_1 + 1) - 1$
		[37]		$2N_2(N_1 + 1) - 2$
		[38]		$6N_2(N_1 + 1) - 4$
	Other	[39]	$M\ +\ M + 2$	-
non-Parallel	L MRA	[40]	$M + N - 1$	-
	L 2 ||	[41]	$4N + 1$	N
	L coprime	[42]	$2M_1 + M_2 - 1$	M_1M_2
		[43]	$4M_1 + 2M_2 - 3$	M_1M_2
	L Nested	[44]	$2N - 1,\ N := N_1 + N_2$	$\begin{cases} 3N^2/2 - 2, & N \text{ even} \\ 3N^2/2 - N - 1/2, & N \text{ odd} \end{cases}$
		[45]		$N^2/4 + N/2 - 1$
		[46]	$N_{x1} + N_{x2} + N_{y1} + N_{y2}$	$(2N_{x1}N_{x2} + 2N_{x2} - 1) \times (2N_{y2}N_{y1} + 2N_{y2} + 2N_{y1} + 1)$
		[47]	$4N_1 - 2$	$4N_1^2 - 2$
		[48]	$2N - 1,\ N := N_1 + N_2$	$0.25(N^2 - 1) + 0.5(N - 1)$
	IA	[49]	$2M + 2N - 1$	$(M + 1)\,(2M + 2N - 1 - M - \lfloor M/2 \rfloor)$
	L sULA+	[50]	$M + 1\ +\ M\ - 1$	-
	L Other	[51]	$M_x + M_z + 1$	-
	VCA	[52]	$2(2M_1 + M_2 - 1) - 1$	M_1N_2
	VNA	[52]	$2N$	$0.25N^2 + N + 2 - 1$
	Cross	[53]	$2M_x + 2M_y + 1$	$\min\{N_x, N_y\}$
	Billboard	[54]	$3(N_x - 1)$	-
	OBA	[54]	$N_x + 2N_y - 2$	$(2N_x - 1) \times (2N_y - 1)$
Planar	CPA	[55]	$M_1^2 + M_2^2$	$\min\{M_1^2, M_2^2\} - 1$
	GCPA	[56]	$M_1N_1 + M_2N_2$	$\min\{M_1N_1, M_2N_2\} - 1$
	CPA	[57]	$M_1^2 + M_2^2 - 1$	$\min\{M_1^2 + M_2^2 - 1 - M_1, M_1^2 + M_2^2 - 1 - M_2\}$
	CPA	[58]	$M_1^2 + M_2^2 - 1$	Check Section IV-A of [58].
	Nested	[59, 60]	$(N_1 + N_2)^2$	Check Table I and Table III of [60].
	Unfolded	[61]	$M_1^2 + M_2^2 - 1$	$M_1^2 + M_2^2 - 2$
	NCPA	[62]	$(L + M_1 - 1)^2 + (L + M_2 - 1)^2 - L^2$	$\min\{(LM_1)^2 - 1, (LM_2)^2 - 1\}$
Other	HOBA-2	[54]	$N_x + 2N_y - 2$	$(2N_x - 1) \times (2N_y - 1)$
	Hourglass	[54]	$N_x + 2N_y - 2$	$(2N_x - 1) \times (2N_y - 1)$
	Thermos	[63]	$N_x + 2N_y - 2$	$(2N_x + 1) \times (2N_y - 3)$
	Concentric	[64]	$2(N_x + N_y)$	-

-: a dash mark signifies that the value is not mentioned directly in the paper, or not easily verifiable.

where $\{1 : 2 : N - 1\} = \{1, 1 + 2, 1 + 4, \ldots, N - 1\}$ is an interval of integers with a step size of 2. The hourglass array is sparser than the CcRA, and both have a contiguous difference coarray. However, the CcRA has a contiguous sum coarray, unlike the hourglass array [64]. In addition, all the elements in the CcRA are essential [19].

IV. COMPARATIVE EVALUATION

This section presents a general comparison of the mentioned arrays and highlights some important differences. This should be useful in predicting the estimation performance and required complexity of a sensor geometry; thus, aiding the decision of selecting a sensor geometry for 2D-DoA estimation. It can also serve as a starting point for researchers interested in exploring or designing new sparse planar arrays in more detail. The comparative evaluation presented in this section is organized in a table split over two pages due to limited space. In other words, Table 2 and Table 3 share the same rows, the same 'Array' and 'Ref.' columns, but have the rest of columns different.

TABLE 3. Comparison between array geometries in terms of computational complexity, mutual coupling, and aperture.

Array		Ref.	PS[1]	FOC	MC-1[2]	Aperture, x	Aperture, y
Parallel	Coprime	[30]	✗	✗	Low	1	$M_2(2M_1-1)$
		[31]	✗	✗	Low	1	$2M_2(2M_1-1)$
		[32]	✓	✗	Low	1	$M_1(M_2-1)$
		[33]	1D	✗	Low	1	$M_1(M_2-1)$
		[34]	✓	✗	Low	1	$M_2(2M_1-1)$
		[35]	1D	✗	Low	$1+L$	$M_2(2M_1-1)$
	Nested	[36]	✗	✗	High	1	$N_2(N_1+1)-1$
		[37]	✗	✗	High	1	$N_2(N_1+1)-1$
		[38]	✗	✓	High	1	$N_2(N_1+1)-1$
	Other	[39]	✗	✗	High	1	$M+1$
non-Parallel	L MRA	[40]	✗	✓	Low	-	-
	L 2 ||	[41]	✗	✗	High	$N-1$	$N-1$
	L coprime	[42]	✗	✗	Low	$M_2(2M_1-1)$	$M_1(M_2-1)$
		[43]	1D	✗	Low	$M_2(2M_1-1)$	$M_2(2M_1-1)$
	L Nested	[44]	✗	✗	High	$N_2(N_1+1)-1$	$N_2(N_1+1)-1$
		[45]	✗	✗	High	$N_2(N_1+1)-1$	$N_2(N_1+1)-1$
		[46]	✗	✓	High	$N_{x2}(N_{x1}+1)-1$	$2N_{y2}(N_{y1}+1)-2$
		[47]	✗	✗	High	$2N_1-1$	$2N_1-1$
		[48]	2D	✗	High	$N_2(N_1+1)-1$	$N_2(N_1+1)-1$
	IA	[49]	1D	✗	Medium	$(M+N-\lfloor M/2\rfloor-2)(M+1)M$	
	L sULA+	[50]	✗	✗	Medium	$M-1$	M
	L Other	[51]	✗	✗	Medium	M_x	M_y
	VCA	[52]	1D	✗	Low	$2M_1(M_2-1)\sin(\Omega/2)$	$M_1(M_2-1)\cos(\Omega/2)$
	VNA	[52]	1D	✗	High	$2(N_2(N_1+1)-1)\sin(\Omega/2)$	$(N_2(N_1+1)-1)\cos(\Omega/2)$
	Cross	[53]	✗	✗	Medium	$2(M_x-1)$	$2(M_y-1)$
	Billboard	[54]	✗	✗	High	N_x-1	N_y-1
	OBA	[54]	✗	✗	High	N_x-1	N_y-1
Planar	CPA	[55]	2D-PSS[3]	✗	Low	$M_1(M_2-1)$	$M_1(M_2-1)$
	GCPA	[56]	2D	✗	Low	$M_1(M_2-1)$	$N_1(N_2-1)$
	CPA	[57]	✗	✗	Low	$M_1(M_2-1)$	$M_1(M_2-1)$
	CPA	[58]	✗	≳[4]	Low	$M_1(M_2-1)$	$M_1(M_2-1)$
	Nested	[59, 60]	2D	✗	High	$N_2(N_1+1)-1$	$N_2(N_1+1)-1$
	Unfolded	[61]	1D	✗	Low	$M_1(M_2-1)+M_2(M_1-1)$	$M_1(M_2-1)+M_2(M_1-1)$
	NCPA	[62]	2D	✗	Medium	$M_1(M_2-1)+M_1M_2(L-1)$	$M_1(M_2-1)+M_1M_2(L-1)$
Other	HOBA-2	[54]	✗	✗	Low	N_x-1	N_y-1
	Hourglass	[54]	✗	✗	Low	N_x-1	N_y-1
	Thermos	[63]	2D	✗	Low	N_x+3	N_y-2
	Concentric	[64]	-	-	Low	N_x	N_y

[1]PS: Peak Search. [2]MC-1:Mutual Coupling approximate classification based on number of elements with unity inter-sensor spacing
[3]PSS: Partial Spectral Search. [4]Means the paper does not propose a method based on FOC, but compares results with a method based on FOC.

Table 2 lists the number of elements in each array geometry and the achievable DOF. For instance, the three papers [36]–[38] that used parallel nested arrays are easily comparable, and the latest one [38] using fourth order cumulants (FOC) has higher DOF as expected. It is not straight forward to compare all types of arrays since many sparse planar arrays are based on coprime, nested, or other linear arrays. In addition, some array geometries have different DOF when the parameters specifying the array are even or odd. In Table 2, a dash signifies that the value is not mentioned directly in the paper, or not easily verifiable. For example, Jian *et al.* [40] uses MRAs which do not have a closed form expression for the physical sensor locations; yet the expression shown for the number of sensors is a mere summation of the elements in the two subarrays (linear arrays). For other works, this could indicate that the work is focused on reducing computational complexity or other improvements apart from increasing DOF.

The arrays are listed in Table 2 based on the classification that was presented in Section III, then chronologically. As such, it is generally expected that, within each category, later papers achieve higher DOF than older ones. As an example, Zheng *et al.* [61] state that their UCPA can exceed the DOF of the earlier works by Wu *et al.* [55] and Zheng *et al.* [56]. Similarly, Si et al. [62] show that their NCPA can exceed the DOF of the previous CPA variants: CPA [55], GCPA [56] and UCPA [61]. Another example is the thermos array [63] which can exceed the DOF of the hourglass array when $N_y > N_x + 1$. Furthermore, another interesting note might be the equal DOF of the arrays: OBA, HOBA-2, and hourglass [54]. In this case, this is an advantage for the newer arrays (HOBA-2 and hourglass), since these arrays retain the hole-free difference coarray of the OBA, yet they reduce mutual coupling.

Table 3 shows a comparison of the same arrays in Table 2, but now shows the aperture, the estimated mutual coupling sensitivity based on the number of sensors with close inter-sensor spacing (MC-1), and whether the paper uses peak search (PS) or FOC which give an indication of the computational complexity. Only three papers considered FOC in the algorithm [38], [40], [46]. This can be explained by the computational complexity of FOC, and the condition that the sources must not be Gaussian. Despite the fact that it theoretically eliminates the Gaussian noise, and usually leads to much larger DOF compared to methods based on order statistics (SOS). However, one paper showed that it is possible to exceed the performance of some FOC-based methods [58]. Further, it can be noted that, in general, array geometries utilizing nested arrays have higher number of sensors closely-spaced, and as such, are more susceptible to mutual coupling degradation. In addition, some of the recent arrays like hourglass or thermos arrays have low mutual coupling sensitivity. Other notes on Table 3 include:

- The column PS only describes the existence of a step in the cited paper. For instance, Qin et al. [35] only employ 1D search in the case of having sources less than sensors, while exploiting sparse learning techniques when the number of sources exceeds the physical sensors.
- It is worth mentioning that comparing the DOF offered by a method using FOC to another method using SOS may not be fair. However, since not all arrays are expected to work well with FOC, and because of the low number of papers using FOC, the papers using FOC are also listed in the same table.
- Not having PS does not mean having lower computational time. For example, Wu and Zhu [53] use atomic norm minimization (ANM) for 2D-DoA estimation, yet they report relatively higher computational time than some other methods. They still, however, employ a MUSIC-like method for range estimation.
- In many cases, it is possible to use different estimation methods. Hence, for some of the works that utilize 2D PS, it could be possible to try a less complicated method. However, the use of such 2D peak searching methods can be justified when the main contribution of the paper is in a different direction, and a baseline comparison is seeked. For example, Sun *et al.* [63] presented the thermos array trying mainly to reduce mutual coupling by spacing some sensors further apart from each other, based on ideas from the hourglass array proposed earlier by Liu and Vaidyanathan [54]. Another example is the work of Zheng *et al.* [56] which mainly presents the GCPA structure that is a generalization of the CPA.
- Using 2D PS is not always the worst in terms of computational complexity. For example, Wu *et al.* [55] used a limited 2D spectral search that is having less complexity than the full 2D search.
- The last two columns show the aperture of the array in the x and y directions. While in general, arrays based on coprime linear arrays for example have the same aperture; some differences exist if authors use different definitions of the coprime linear array, or if the linear array on the x and y directions are different. Similar arguments apply to other linear arrays. Note that it is not easy to write an expression for the aperture if the linear array (LA) is a minimum redundancy array (MRA). In addition, sometimes $N_x - 1$ is the aperture of the array by design like hourglass and HOBA-2. In addition, if ULAs are used, the table shows the number of elements in the ULA on that axis. In many cases, the aperture is square and the same expression appear in both columns. However, for the work by Wu et al. [49], the expression is made to span both columns to save space.

V. CONCLUDING REMARKS

The increased number of location-based services and applications has led to increased interest in 2D sparse arrays which enable localization with minimum number of sensors. Published research efforts are not fully aligned and do not fall under clear framework. In this paper, we presented a comprehensive and structured literature overview of sparse arrays for 2D-DoA estimation. Popular designs like L-shaped, V-shaped, hourglass, thermos, nested planar, and coprime planar were classified into parallel arrays, non-parallel arrays, and other planar arrays. Existing designs were compared in terms of the required number of sensors, DOF, algorithm used, complexity and aperture size. A fair comparison should not overlook the aperture size associated with the improved estimation performance. L-shaped sparse arrays received the largest attention in the literature. However, other new structures seem promising. Arrays with rectangular aperture tend to show large DOF, like the hourglass or thermos arrays. Also, GCPA show large DOF compared to CPA. Arrays with relatively more complicated closed-form expressions seem to enjoy more DOF, like the hourglass or thermos arrays.

While the emphasis was on the 2D sparse arrays' structure, some designs require modified DoA estimation algorithms. Many algorithms for 2D-DoA estimation employ vectorization of cross correlation matrix, and then progress by various minimization methods. Some do spatial smoothing, and

others avoid it to evade reduction in available DOF. Performance metrics of 2D-DoA estimation were outlined and existing solutions to alleviate problems were discussed. The presented structured review should help in predicting the DoA estimation performance and required complexity; thus, facilitating design and selection of sensor array geometry for 2D-DoA estimation.

REFERENCES

[1] H. Krim and M. Viberg, "Two decades of array signal processing research: The parametric approach," *IEEE Signal Process. Mag.*, vol. 13, no. 4, pp. 67–94, Jul. 1996.

[2] M. Xiao, S. Mumtaz, Y. Huang, L. Dai, Y. Li, M. Matthaiou, G. K. Karagiannidis, E. Björnson, K. Yang, C.-L. I, and A. Ghosh, "Millimeter wave communications for future mobile networks," *IEEE J. Sel. Areas Commun.*, vol. 35, no. 9, pp. 1909–1935, Sep. 2017.

[3] E. Björnson, L. Sanguinetti, H. Wymeersch, J. Hoydis, and T. L. Marzetta, "Massive MIMO is a reality—What is next?: Five promising research directions for antenna arrays," *Digit. Signal Process.*, vol. 94, pp. 3–20, Nov. 2019.

[4] A. Fascista, A. Coluccia, H. Wymeersch, and G. Seco-Granados, "Millimeter-wave downlink positioning with a single-antenna receiver," *IEEE Trans. Wireless Commun.*, vol. 18, no. 9, pp. 4479–4490, Sep. 2019.

[5] S. DeGraaf and D. Johnson, "Optimal linear arrays for narrow-band beamforming," in *Proc. IEEE Int. Conf. Acoust., Speech, Signal Process. (ICASSP)*, vol. 9, Mar. 1984, pp. 214–217.

[6] Y. Bresler and A. Macovski, "On the number of signals resolvable by a uniform linear array," *IEEE Trans. Acoust., Speech, Signal Process.*, vol. ASSP-34, no. 6, pp. 1361–1375, Dec. 1986.

[7] M. P. Wylie, S. Roy, and H. Messer, "Joint DOA estimation and phase calibration of linear equispaced (LES) arrays," *IEEE Trans. Signal Process.*, vol. 42, no. 12, pp. 3449–3459, Dec. 1994.

[8] B. Porat and B. Friedlander, "Direction finding algorithms based on high-order statistics," *IEEE Trans. Signal Process.*, vol. 39, no. 9, pp. 2016–2024, Sep. 1991.

[9] A. Swami and J. M. Mendel, "Cumulant-based approach to harmonic retrieval and related problems," *IEEE Trans. Signal Process.*, vol. 39, no. 5, pp. 1099–1109, May 1991.

[10] A. Moffet, "Minimum-redundancy linear arrays," *IEEE Trans. Antennas Propag.*, vol. AP-16, no. 2, pp. 172–175, Mar. 1968.

[11] D. A. Linebarger, "A fast method for computing the coarray of sparse linear arrays," *IEEE Trans. Antennas Propag.*, vol. 40, no. 9, pp. 1109–1112, Sep. 1992.

[12] S. D. Bedrosian, "Nonuniform linear arrays: Graph-theoretic approach to minimum redundancy," *Proc. IEEE*, vol. 74, no. 7, pp. 1040–1043, Jul. 1986.

[13] D. A. Linebarger, I. H. Sudborough, and I. G. Tollis, "Difference bases and sparse sensor arrays," *IEEE Trans. Inf. Theory*, vol. 39, no. 2, pp. 716–721, Mar. 1993.

[14] P. Pal and P. P. Vaidyanathan, "Coprime sampling and the music algorithm," in *Proc. Digit. Signal Process. Signal Process. Educ. Meeting (DSP/SPE)*, Jan. 2011, pp. 289–294.

[15] S. Qin, Y. D. Zhang, and M. G. Amin, "Generalized coprime array configurations for direction-of-arrival estimation," *IEEE Trans. Signal Process.*, vol. 63, no. 6, pp. 1377–1390, Mar. 2015.

[16] S. A. Alawsh and A. H. Muqaibel, "Sparse DOA estimation based on multi-level prime array with compression," *IEEE Access*, vol. 7, pp. 70828–70841, 2019.

[17] P. Pal and P. P. Vaidyanathan, "Nested arrays: A novel approach to array processing with enhanced degrees of freedom," *IEEE Trans. Signal Process.*, vol. 58, no. 8, pp. 4167–4181, Aug. 2010.

[18] C.-L. Liu and P. P. Vaidyanathan, "Super nested arrays: Linear sparse arrays with reduced mutual coupling—Part I: Fundamentals," *IEEE Trans. Signal Process.*, vol. 64, no. 15, pp. 3997–4012, Aug. 2016.

[19] C.-L. Liu and P. P. Vaidyanathan, "Maximally economic sparse arrays and cantor arrays," in *Proc. IEEE 7th Int. Workshop Comput. Adv. Multi-Sensor Adapt. Process. (CAMSAP)*, Dec. 2017, pp. 1–5.

[20] R. Rajamäki and V. Koivunen, "Comparison of sparse sensor array configurations with constrained aperture for passive sensing," in *Proc. IEEE Radar Conf. (RadarConf)*, May 2017, pp. 0797–0802.

[21] S. Mazlout, M. B. Ben Salah, and A. Samet, "Comparative study of two array configurations for 2D-DOA estimation in LS-MIMO systems," in *Proc. 6th Int. Conf. Commun. Netw. (ComNet)*, Mar. 2017, pp. 1–6.

[22] A. B. Gershman, M. Rübsamen, and M. Pesavento, "One- and two-dimensional direction-of-arrival estimation: An overview of search-free techniques," *Signal Process.*, vol. 90, no. 5, pp. 1338–1349, May 2010.

[23] A. M. Zoubir, V. Koivunen, Y. Chakhchoukh, and M. Muma, "Robust estimation in signal processing: A tutorial-style treatment of fundamental concepts," *IEEE Signal Process. Mag.*, vol. 29, no. 4, pp. 61–80, Jul. 2012.

[24] S. Kiani and A. M. Pezeshk, "A comparative study of several array geometries for 2D DOA estimation," *Procedia Comput. Sci.*, vol. 58, pp. 18–25, Jan. 2015.

[25] S. Khedekar and M. Mukhopadhyay, "Analysis of estimation of direction of arrival by comparative study," *Mater. Today, Proc.*, vol. 5, no. 1, pp. 1696–1703, 2018.

[26] A. Ahmed, S. A. Hamza, and M. Tufail, "Comparative analysis of fourth order cumulant based ESPRIT algorithms," in *Proc. 12th Int. Conf. Frontiers Inf. Technol.*, Dec. 2014, pp. 133–138.

[27] K. Adhikari and B. Drozdenko, "Comparison of MUSIC variants for sparse arrays," in *Proc. IEEE Nat. Aerosp. Electron. Conf. (NAECON)*, Jul. 2019, pp. 398–405.

[28] Q. Shen, W. Liu, W. Cui, and S. Wu, "Underdetermined DOA estimation under the compressive sensing framework: A review," *IEEE Access*, vol. 4, pp. 8865–8878, 2016.

[29] Y. Liang, W. Liu, Q. Shen, W. Cui, and S. Wu, "A review of closed-form Cramér-Rao bounds for DOA estimation in the presence of Gaussian noise under a unified framework," *IEEE Access*, vol. 8, pp. 175101–175124, 2020.

[30] S. Qin, Y. D. Zhang, and M. G. Amin, "Two-dimensional DOA estimation using parallel coprime subarrays," in *Proc. IEEE Sensor Array Multichannel Signal Process. Workshop (SAM)*, Jul. 2016, pp. 1–4.

[31] J. Shi, G. Hu, X. Zhang, and P. Gong, "Sum and difference coarrays based 2-D DOA estimation with co-prime parallel arrays," in *Proc. 9th Int. Conf. Wireless Commun. Signal Process. (WCSP)*, Oct. 2017, pp. 1–4.

[32] F. Sun, P. Lan, B. Gao, and G. Zhang, "An efficient dictionary learning-based 2-D DOA estimation without pair matching for co-prime parallel arrays," *IEEE Access*, vol. 6, pp. 8510–8518, 2018.

[33] F. Sun, S. Ouyang, P. Lan, and F. Li, "Reduced dimensional 2-D DOA estimation via least partial search with automatic pairing for parallel co-prime arrays," in *Proc. IEEE 11th Sensor Array Multichannel Signal Process. Workshop (SAM)*, Jun. 2020, pp. 1–5.

[34] P. Gong, X. Zhang, J. Shi, and W. Zheng, "Three-parallel co-prime array configuration for two-dimensional DOA estimation," in *Proc. 9th Int. Conf. Wireless Commun. Signal Process. (WCSP)*, Oct. 2017, pp. 1–5.

[35] S. Qin, Y. D. Zhang, and M. G. Amin, "Improved two-dimensional DOA estimation using parallel coprime arrays," *Signal Process.*, vol. 172, Jul. 2020, Art. no. 107428.

[36] X. Li, W. Zhang, T. Shu, and J. He, "Two-dimensional direction finding with parallel nested arrays using DOA matrix method," *IEEE Sensors Lett.*, vol. 3, no. 7, pp. 1–4, Jul. 2019.

[37] Z. Zheng and S. Mu, "Two-dimensional DOA estimation using two parallel nested arrays," *IEEE Commun. Lett.*, vol. 24, no. 3, pp. 568–571, Mar. 2020.

[38] J. He, L. Li, and T. Shu, "2-D direction finding using parallel nested arrays with full co-array aperture extension," *Signal Process.*, vol. 178, Jan. 2021, Art. no. 107795.

[39] Z. Zheng, Y. Yang, W.-Q. Wang, and S. Zhang, "Two-dimensional direction estimation of multiple signals using two parallel sparse linear arrays," *Signal Process.*, vol. 143, pp. 112–121, Feb. 2018.

[40] C. Jian, S. Wang, and L. Lin, "2-D DOA estimation by minimum-redundancy linear array," in *Proc. 8th Int. Conf. Signal Process.*, vol. 1, Nov. 2006. [Online]. Available: https://ieeexplore.ieee.org/document/4128862

[41] J. He and Z. Liu, "Extended aperture 2-D direction finding with a two-parallel-shape-array using propagator method," *IEEE Antennas Wireless Propag. Lett.*, vol. 8, pp. 323–327, 2009.

[42] Q. Liu, X. Yi, L. Jin, and W. Chen, "Two dimensional direction of arrival estimation for co-prime L-shaped array using sparse reconstruction," in *Proc. 8th Int. Congr. Image Signal Process. (CISP)*, Oct. 2015, pp. 1499–1503.

[43] A. M. Elbir, "L-shaped coprime array structures for DOA estimation," *Multidimensional Syst. Signal Process.*, vol. 31, no. 1, pp. 205–219, Jan. 2020.

[44] Y.-Y. Dong, C.-X. Dong, Y.-T. Zhu, G.-Q. Zhao, and S.-Y. Liu, "Two-dimensional DOA estimation for L-shaped array with nested subarrays without pair matching," *IET Signal Process.*, vol. 10, pp. 1112–11175, Dec. 2016.
[45] C. Niu, Y. Zhang, and J. Guo, "Interlaced double-precision 2-D angle estimation algorithm using L-shaped nested arrays," *IEEE Signal Process. Lett.*, vol. 23, no. 4, pp. 522–526, Apr. 2016.
[46] X. Li, S. Ren, J. Liu, and W. Wang, "Augmented L-shaped nested array based on the fourth-order difference co-array concept," in *Proc. IEEE 10th Sensor Array Multichannel Signal Process. Workshop (SAM)*, Jul. 2018, pp. 31–35.
[47] X. Gao, X. Hao, P. Li, and G. Li, "An improved two-dimensional direction-of-arrival estimation algorithm for L-shaped nested arrays with small sample sizes," *Sensors*, vol. 19, no. 9, p. 2176, May 2019.
[48] Y. Yang, X. Mao, Y. Hou, and G. Jiang, "2-D DOA estimation via correlation matrix reconstruction for nested L-shaped array," *Digit. Signal Process.*, vol. 98, Mar. 2020, Art. no. 102623.
[49] F. Wu, F. Cao, X. Ni, C. Chen, Y. Zhang, and J. Xu, "L-shaped sparse array structure for 2-D DOA estimation," *IEEE Access*, vol. 8, pp. 140030–140037, 2020.
[50] Y. Yang, Z. Zheng, H. Yang, J. Yang, and Y. Ge, "A novel 2-D DOA estimation method via sparse L-shaped array," in *Proc. 2nd IEEE Int. Conf. Comput. Commun. (ICCC)*, Oct. 2016, pp. 1865–1869.
[51] J.-F. Gu, W.-P. Zhu, and M. N. S. Swamy, "Joint 2-D DOA estimation via sparse L-shaped array," *IEEE Trans. Signal Process.*, vol. 63, no. 5, pp. 1171–1182, Mar. 2015.
[52] A. M. Elbir, "V-shaped sparse arrays for 2-D DOA estimation," *Circuits, Syst., Signal Process.*, vol. 38, no. 6, pp. 2792–2809, Jun. 2019.
[53] X. Wu and W.-P. Zhu, "Single far-field or near-field source localization with sparse or uniform cross array," *IEEE Trans. Veh. Technol.*, vol. 69, no. 8, pp. 9135–9139, Aug. 2020.
[54] C.-L. Liu and P. P. Vaidyanathan, "Hourglass arrays and other novel 2-D sparse arrays with reduced mutual coupling," *IEEE Trans. Signal Process.*, vol. 65, no. 13, pp. 3369–3383, Jul. 2017.
[55] Q. Wu, F. Sun, P. Lan, G. Ding, and X. Zhang, "Two-dimensional direction-of-arrival estimation for co-prime planar arrays: A partial spectral search approach," *IEEE Sensors J.*, vol. 16, no. 14, pp. 5660–5670, Jul. 2016.
[56] W. Zheng, X. Zhang, and H. Zhai, "Generalized coprime planar array geometry for 2-D DOA estimation," *IEEE Commun. Lett.*, vol. 21, no. 5, pp. 1075–1078, May 2017.
[57] D. Zhang, Y. Zhang, G. Zheng, B. Deng, C. Feng, and J. Tang, "Two-dimensional direction of arrival estimation for coprime planar arrays via polynomial root finding technique," *IEEE Access*, vol. 6, pp. 19540–19549, 2018.
[58] H. Xu, D. Wang, B. Ba, W. Cui, and Y. Zhang, "Direction-of-arrival estimation for both uncorrelated and coherent signals in coprime array," *IEEE Access*, vol. 7, pp. 18590–18600, 2019.
[59] P. Pal and P. P. Vaidyanathan, "Nested arrays in two dimensions, Part I: Geometrical considerations," *IEEE Trans. Signal Process.*, vol. 60, no. 9, pp. 4694–4705, Sep. 2012.
[60] P. Pal and P. P. Vaidyanathan, "Nested arrays in two dimensions, Part II: Application in two dimensional array processing," *IEEE Trans. Signal Process.*, vol. 60, no. 9, pp. 4706–4718, Sep. 2012.
[61] W. Zheng, X. Zhang, L. Xu, and J. Zhou, "Unfolded coprime planar array for 2D direction of arrival estimation: An aperture-augmented perspective," *IEEE Access*, vol. 6, pp. 22744–22753, 2018.
[62] W. Si, F. Zeng, Z. Qu, and Z. Peng, "Two-dimensional DOA estimation via a novel sparse array consisting of coprime and nested subarrays," *IEEE Commun. Lett.*, vol. 24, no. 6, pp. 1266–1270, Jun. 2020.
[63] L. Sun, M. Yang, and B. Chen, "Thermos array: Two-dimensional sparse array with reduced mutual coupling," *Int. J. Antennas Propag.*, vol. 2018, pp. 1–8, Jan. 2018.
[64] R. Rajamäki and V. Koivunen, "Sparse active rectangular array with few closely spaced elements," *IEEE Signal Process. Lett.*, vol. 25, no. 12, pp. 1820–1824, Dec. 2018.
[65] A. J. van der Veen, P. B. Ober, and E. F. Deprettere, "Azimuth and elevation computation in high resolution DOA estimation," *IEEE Trans. Signal Process.*, vol. 40, no. 7, pp. 1828–1832, Jul. 1992.
[66] J. Liang and D. Liu, "Joint elevation and azimuth direction finding using L-shaped array," *IEEE Trans. Antennas Propag.*, vol. 58, no. 6, pp. 2136–2141, Jun. 2010.
[67] R. Schmidt, "Multiple emitter location and signal parameter estimation," *IEEE Trans. Antennas Propag.*, vol. AP-34, no. 3, pp. 276–280, Mar. 1986.
[68] R. Roy and T. Kailath, "ESPRIT-estimation of signal parameters via rotational invariance techniques," *IEEE Trans. Acoust., Speech, Signal Process.*, vol. 37, no. 7, pp. 984–995, Jul. 1989.
[69] S. Marcos, A. Marsal, and M. Benidir, "The propagator method for source bearing estimation," *Signal Process.*, vol. 42, no. 2, pp. 121–138, Mar. 1995.
[70] Z. Ye and C. Liu, "2-D DOA estimation in the presence of mutual coupling," *IEEE Trans. Antennas Propag.*, vol. 56, no. 10, pp. 3150–3158, Oct. 2008.
[71] H. Chen, C. Hou, W.-P. Zhu, W. Liu, Y.-Y. Dong, Z. Peng, and Q. Wang, "ESPRIT-like two-dimensional direction finding for mixed circular and strictly noncircular sources based on joint diagonalization," *Signal Process.*, vol. 141, pp. 48–56, Dec. 2017.
[72] C.-H. Lin, W.-H. Fang, J.-D. Lin, and K.-H. Wu, "A fast algorithm for joint two-dimensional direction of arrival and frequency estimation via hierarchical space–time decomposition," *Signal Process.*, vol. 90, no. 1, pp. 207–216, Jan. 2010.
[73] Y. Wu, G. Liao, and H. C. So, "A fast algorithm for 2-D direction-of-arrival estimation," *Signal Process.*, vol. 83, no. 8, pp. 1827–1831, Aug. 2003.
[74] J. Li, X. Zhang, and H. Chen, "Improved two-dimensional DOA estimation algorithm for two-parallel uniform linear arrays using propagator method," *Signal Process.*, vol. 92, no. 12, pp. 3032–3038, Dec. 2012.
[75] P. Li, B. Yu, and J. Sun, "A new method for two-dimensional array signal processing in unknown noise environments," *Signal Process.*, vol. 47, no. 3, pp. 319–327, Dec. 1995.
[76] Y. Zhang, X. Xu, Y. A. Sheikh, and Z. Ye, "A rank-reduction based 2-D DOA estimation algorithm for three parallel uniform linear arrays," *Signal Process.*, vol. 120, pp. 305–310, Mar. 2016.
[77] R. T. Hoctor and S. A. Kassam, "The unifying role of the coarray in aperture synthesis for coherent and incoherent imaging," *Proc. IEEE*, vol. 78, no. 4, pp. 735–752, Apr. 1990.
[78] C. Zhu, W.-Q. Wang, H. Chen, and H. C. So, "Impaired sensor diagnosis, beamforming, and DOA estimation with difference co-array processing," *IEEE Sensors J.*, vol. 15, no. 7, pp. 3773–3780, Jul. 2015.
[79] B. Friedlander, "Antenna array manifolds for high-resolution direction finding," *IEEE Trans. Signal Process.*, vol. 66, no. 4, pp. 923–932, Feb. 2018.
[80] H. Huang, M. Fauß, and A. M. Zoubir, "Block sparsity-based DOA estimation with sensor gain and phase uncertainties," in *Proc. 27th Eur. Signal Process. Conf. (EUSIPCO)*, Sep. 2019, pp. 1–5.
[81] C.-L. Liu and P. P. Vaidyanathan, "Robustness of difference coarrays of sparse arrays to sensor failures—Part I: A theory motivated by coarray MUSIC," *IEEE Trans. Signal Process.*, vol. 67, no. 12, pp. 3213–3226, Jun. 2019.
[82] C.-L. Liu and P. P. Vaidyanathan, "Robustness of difference coarrays of sparse arrays to sensor failures—Part II: Array geometries," *IEEE Trans. Signal Process.*, vol. 67, no. 12, pp. 3227–3242, Jun. 2019.
[83] Y. I. Abramovich, D. A. Gray, A. Y. Gorokhov, and N. K. Spencer, "Positive-definite Toeplitz completion in DOA estimation for nonuniform linear antenna arrays. I. Fully augmentable arrays," *IEEE Trans. Signal Process.*, vol. 46, no. 9, pp. 2458–2471, Sep. 1998.
[84] S. Orfanidis, *Electromagnetic Waves and Antennas*. 2016. [Online]. Available: https://www.ece.rutgers.edu/~orfanidi/ewa/
[85] B. Friedlander and A. J. Weiss, "Direction finding in the presence of mutual coupling," *IEEE Trans. Antennas Propag.*, vol. 39, no. 3, pp. 273–284, Mar. 1991.
[86] T. Jiang, N. D. Sidiropoulos, and J. M. F. ten Berge, "Almost-sure identifiability of multidimensional harmonic retrieval," *IEEE Trans. Signal Process.*, vol. 49, no. 9, pp. 1849–1859, Sep. 2001.
[87] A. Agarwal, M. Agrawal, and A. Kumar, "Higher-order-statistics-based direction-of-arrival estimation of multiple wideband sources with single acoustic vector sensor," *IEEE J. Ocean. Eng.*, vol. 45, no. 4, pp. 1439–1449, Oct. 2020.
[88] K. Adhikari and B. Drozdenko, "Symmetry-imposed rectangular coprime and nested arrays for direction of arrival estimation with multiple signal classification," *IEEE Access*, vol. 7, pp. 153217–153229, 2019.
[89] H. Chen, C.-P. Hou, Q. Wang, L. Huang, and W.-Q. Yan, "Cumulants-based Toeplitz matrices reconstruction method for 2-D coherent DOA estimation," *IEEE Sensors J.*, vol. 14, no. 8, pp. 2824–2832, Aug. 2014.

[90] S. Liu, L. S. Yang, D. C. Wu, and J. H. Huang, "Two-dimensional DOA estimation using a co-prime symmetric cross array," *PIER C*, vol. 54, pp. 67–74, Oct. 2014, doi: 10.2528/PIERC14081005.
[91] S. Sekizawa, "Estimation of arrival directions using MUSIC algorithm with a planar array," in *Proc. IEEE Int. Conf. Universal Pers. Commun. Conf. (ICUPC)*, vol. 1, Oct. 1998, pp. 555–559.
[92] T.-J. Shan, M. Wax, and T. Kailath, "On spatial smoothing for direction-of-arrival estimation of coherent signals," *IEEE Trans. Acoust., Speech, Signal Process.*, vol. ASSP-33, no. 4, pp. 806–811, Aug. 1985.
[93] Q. Y. Yin, R. W. Newcomb, and L. H. Zou, "Estimating 2-D angles of arrival via two parallel linear arrays," in *Proc. Int. Conf. Acoust., Speech, Signal Process.*, vol. 4, May 1989, pp. 2803–2806.
[94] Q.-Y. Yin, R. W. Newcomb, S. Munjal, and L.-H. Zou, "Relation between the DOA matrix method and the ESPRIT method," in *Proc. IEEE Int. Symp. Circuits Syst.*, vol. 2, May 1990, pp. 1561–1564.
[95] X. Dai, X. Zhang, and Y. Wang, "Extended DOA-matrix method for DOA estimation via two parallel linear arrays," *IEEE Commun. Lett.*, vol. 23, no. 11, pp. 1981–1984, Nov. 2019.
[96] P. P. Vaidyanathan and P. Pal, "Sparse sensing with coprime arrays," in *Proc. Conf. Rec. 44th Asilomar Conf. Signals, Syst. Comput.*, Nov. 2010, pp. 1405–1409.
[97] P. P. Vaidyanathan and P. Pal, "Direct-MUSIC on sparse arrays," in *Proc. Int. Conf. Signal Process. Commun. (SPCOM)*, Jul. 2012, pp. 1–5.
[98] Y. Hua, T. K. Sarkar, and D. D. Weiner, "An L-shaped array for estimating 2-D directions of wave arrival," *IEEE Trans. Antennas Propag.*, vol. 39, no. 2, pp. 143–146, Feb. 1991.
[99] J. He, M. N. S. Swamy, and M. O. Ahmad, "Efficient application of MUSIC algorithm under the coexistence of far-field and near-field sources," *IEEE Trans. Signal Process.*, vol. 60, no. 4, pp. 2066–2070, Apr. 2012.

IBRAHIM ABOUMAHMOUD received the B.Sc. and M.Sc. degrees from the King Fahd University of Petroleum and Minerals (KFUPM), Dhahran, Saudi Arabia, in 2019 and 2021, respectively. His main research interests include signal processing and direction-of-arrival estimation.

ALI MUQAIBEL (Senior Member, IEEE) received the B.Sc. and M.Sc. degrees from the King Fahd University of Petroleum and Minerals (KFUPM), Dhahran, Saudi Arabia, in 1996 and 1999, respectively, and the Ph.D. degree from the Virginia Polytechnic Institute and State University, Blacksburg, VA, USA, in 2003. During his study at Virginia Tech, he was with the Time Domain and RF Measurements Laboratory and the Mobile and Portable Radio Research Group. He was a Visiting Associate Professor with the Center of Advanced Communications, Villanova University, Villanova, PA, USA, in 2013, a Visiting Professor with the Georgia Institute of Technology, in 2015, and a Visiting Scholar with the King Abdullah University for Science and Technology (KAUST), Thuwal, Saudi Arabia, from 2018 to 2019. He is currently a Professor with the Electrical Engineering Department, KFUPM. He is also the Director of the Center for Communication Systems and Sensing. He has authored two book chapters and over 130 articles. His research interests include direction of arrival estimation, through-wall-imaging, localization, channel characterization, and ultra-wideband signal processing. He was a recipient of many awards in the excellence in teaching, advising, and instructional technology.

MOHAMMAD ALHASSOUN (Member, IEEE) received the B.Sc. degree in electrical engineering from the King Fahd University of Petroleum and Minerals (KFUPM), Saudi Arabia, in 2013, and the M.S. and Ph.D. degrees from the Georgia Institute of Technology, Atlanta, GA, USA, in 2015 and 2019, respectively. He has worked at Nokia Bell Labs as an EMCD Intern and a Graduate Assistant at KFUPM, where he was awarded the Best Laboratory Instructor with the Department of Electrical Engineering. He is currently an Assistant Professor with KFUPM. His research interests include radio-channel modeling, retrodirective backscatter communications, spectrally efficient backscatter systems, and physical-layer applications of machine learning. He was a recipient of both the 2018 and 2019 IEEE International Conference on RFID Best Paper Award. He was also awarded the Tech to Teaching Certificate from the College Teaching, Georgia Institute of Technology, and the Associate Level Certificate from the Center of the Integration of Research, Teaching, and Learning.

SALEH ALAWSH (Member, IEEE) received the B.Sc. degree in electronic and communications from Hadhramout University, Al Mukalla, Yemen, in 2007, and the M.Sc. degree in telecommunication and the Ph.D. degree from the King Fahd University of Petroleum and Minerals (KFUPM), Dhahran, Saudi Arabia, in 2013 and 2018, respectively. He joined the Electrical Engineering Department, KFUPM, as a Lecturer, in 2013. His research interests include ultra-wideband systems, narrow band interference mitigation, direction-of-arrival estimation, localization, and compressive sensing.